Journal of Power Sources 208 (2012) 210–224

Contents lists available at SciVerse ScienceDirect

Journal of Power Sources

journal homepage: www.elsevier.com/locate/jpowsour

Review

Thermal runaway caused fire and explosion of lithium ion battery

Qingsong Wang[a,*], Ping Ping[a], Xuejuan Zhao[a], Guanquan Chu[b], Jinhua Sun[a,*], Chunhua Chen[c]

[a] State Key Laboratory of Fire Science, University of Science and Technology of China, Hefei 230026, PR China
[b] Waterborne Transportation Institute, Ministry of Transport, Beijing 100088, PR China
[c] Department of Materials Science & Engineering, University of Science and Technology of China, Hefei 230026, PR China

ARTICLE INFO

Article history:
Received 5 January 2012
Received in revised form 11 February 2012
Accepted 13 February 2012
Available online 22 March 2012

Keywords:
Lithium ion battery
Thermal runaway
Thermal model
Fire prevention

ABSTRACT

Lithium ion battery and its safety are taken more consideration with fossil energy consuming and the reduction requirement of CO_2 emission. The safety problem of lithium ion battery is mainly contributed by thermal runaway caused fire and explosion. This paper reviews the lithium ion battery hazards, thermal runaway theory, basic reactions, thermal models, simulations and experimental works firstly. The general theory is proposed and detailed reactions are summarized, which include solid electrolyte interface decomposition, negative active material and electrolyte reaction, positive active material and electrolyte reaction, electrolyte decomposition, negative active material and binder reaction, and so on. The thermal models or electrochemical–thermal models include one, two and three dimensional models, which can be simulated by finite element method and finite volume method. And then the related prevention techniques are simply summarized and discussed on the inherent safety methods and safety device methods. Some perspectives and outlooks on safety enhancement for lithium ion battery are proposed for the future development.

Contents

* Corresponding authors. Tel.: +86 551 360 6455/6425; fax: +86 551 360 1669.
E-mail addresses: pinew@ustc.edu.cn (Q. Wang), sunjh@ustc.edu.cn (J. Sun).

0378-7753/$ – see front matter © 2012 Elsevier B.V. All rights reserved.
doi:10.1016/j.jpowsour.2012.02.038

1. Introduction

For far too long we have been dependent on fossil fuels to heat our homes, to power our industries, and for transportation. However, the present energy economy based on fossil fuels is facing serious issues [1]. Fossil fuels are a nonrenewable resource, and they take millions of years to develop under extreme conditions. Once they are gone, they can no longer be part of our energy mix. Fossil fuels' downfall is their environmental impact. The burning of fossil fuels is blamed for emissions that contribute to global climate change, acid rain, and ozone problems [2].

The urgency for energy renewal requires the use of clean energy sources at a much higher level than that presently in force. There are new technologies under development that could make burning fossil fuels much more efficient and much cleaner. These technologies could keep fossil fuels in the energy mix for longer but ultimately alternatives must be found.

Accordingly, measures are being adopted in a variety of different fields to help prevent global warming by reducing CO_2 emissions. Investments for the exploitation of renewable energy resources are increasing worldwide, with particular attention to wind and solar power energy plants. In CO_2 emission aspect, the automotive industry has become a focal point when considering impact on the environment. More importantly, advances in environmental technology, such as the emergence of hybrid electric vehicles (HEVs) in the 1990s, have brought innovation to an era where vehicles have been traditionally powered by gasoline. The key feature of hybrid technology is surrounded by the augmentation of the engine with an electric motor, ultimately achieving improved fuel economy and significantly reducing the amount of CO_2 produced by the burning of fuel.

The ongoing challenge of integrating and balancing intermittent renewable energy sources including load leveling, back-up power, grid regulation, and line efficiencies, have created the need for innovation in energy storage. As more renewable energy sources are integrated into the smart grid, managing and storing energy is essential, in particular, large-scale diurnal storage.

Lithium ion battery (LIB) as a kind of new energy is getting more and more attention due to the worldwide energy shortage [3]. Lithium ion batteries are mainly made of electrolyte and active materials, which comprise a very promising energy storage medium for electric and hybrid electric vehicles compared to other energy storage approaches. Because of their lightness and high energy density, lithium ion batteries are ideal for portable devices, such as laptops. In addition, lithium ion batteries have no memory effect and do not use poisonous metals, such as lead, mercury or cadmium. However, these batteries have not been widely deployed commercially in these vehicles yet due to safety, cost, and poor low temperature performance, which are all challenges related to battery thermal management [4–6].

The purpose of this review is to report the state of the art on lithium ion battery safety and related thermal runaway prevention techniques. The first part is about the lithium ion battery thermal runaway mechanism, in which the basic theories, thermal reactions, thermal models and the related progresses on simulation and experiments were summarized. The second part is about how to improve the battery safety or how to prevent the thermal runaway. The measures are basic divided into inherent safety methods and extra safety devices. At last, some possible developments were prospected.

2. Basic concept of lithium ion battery

The three primary functional components of a lithium ion battery are the anode, cathode, and electrolyte. The anode of a conventional lithium ion cell is made from carbon, the cathode is a metal oxide, and the electrolyte is a lithium salt in an organic solvent. The most commercially popular anode material is graphite. The cathode is generally one of three materials: a layered oxide (such as lithium cobalt oxide), a polyanion (such as lithium iron phosphate), or a spinel (such as lithium manganese oxide). The electrolyte is typically a mixture of organic carbonates such as ethylene carbonate (EC) or diethyl carbonate (DEC) containing complexes of lithium ions. These non-aqueous electrolytes generally use non-coordinating anion salts such as lithium hexafluorophosphate ($LiPF_6$), lithium hexafluoroarsenate monohydrate ($LiAsF_6$), lithium perchlorate ($LiClO_4$), and lithium tetrafluoroborate ($LiBF_4$). A separator is necessary to separate the anode and cathode. The separator is a very thin sheet of micro-perforated plastic. It is located between the cathode and the anode and separates the positive and negative electrodes while allowing ions to pass through.

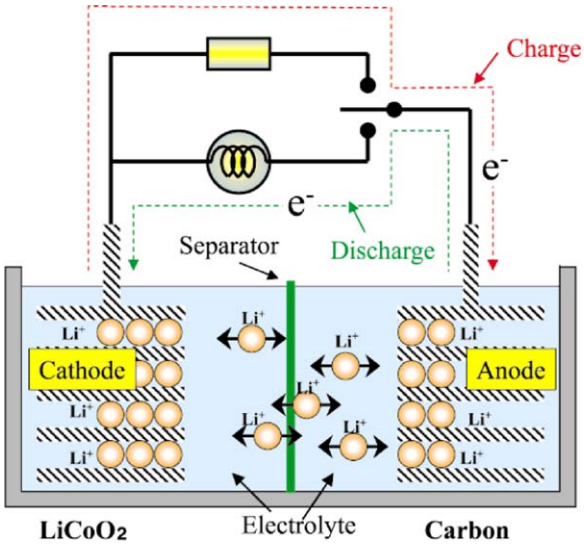

Fig. 1. Schematic of the principle of LIB.
Adopted from Ref. [7].

When a lithium ion battery is charged, lithium ions move from its cathode to its anode, while electrons flow in through an external electrical circuit. The process is reversed during discharge, as shown in Fig. 1 [7]. A lithium ion battery is also known as a swing battery or rocking chair battery since two-way movement of lithium ions between anode and cathode through the electrolyte occurs during charge and discharge process [8]. The more lithium the electrodes can take in, the more total energy the battery can store, and the longer it can last. Most types of batteries are based on the $C/LiPF_6$ in EC–DMC/$LiMO_2$ sequence and operate on a process [2,9]:

The cathode half-reaction is :

$$LiMO_2 \underset{\text{discharge}}{\overset{\text{charge}}{\rightleftarrows}} Li_{1-x}MO_2 + xLi^+ + xe$$

The anode half-reaction is : $$nC + xLi^+ + xe \underset{\text{discharge}}{\overset{\text{charge}}{\rightleftarrows}} Li_xC_n$$

Full cell reaction is : $$LiMO_2 + nC \underset{\text{discharge}}{\overset{\text{charge}}{\rightleftarrows}} Li_{1-x}MO_2 + Li_xC_n$$

where M is Co, Ni, Fe, W, etc., and the cathode materials may be $LiCoO_2$, $LiNiO_2$, $LiMn_2O_4$, $LiFeO_2$, $LiWO_2$. The anode materials may be Li_xC_6, TiS_2, WO_3, NbS_2, V_2O_5, etc.

Table 1
Some lithium ion battery fire and explosion accidents in the past few years.

No.	Date	Accidents replay	Fire causes
1	18 July, 2011	EV bus catch fire, Shanghai, China	Caused by overheated $LiFePO_4$ batteries
2	11 April, 2011	EV taxi catch fire, Hangzhou, China	Caused by 16 Ah $LiFePO_4$ battery
3	3 September, 2010	A Boeing B747-400F cargo plane catch fire, Dubai	Caused by overheated lithium batteries
4	26 April, 2010	Acer recalled 2700 laptop batteries, as Dell, Apple, Toshiba, Lenovo and Sony done in 2006	Potential overheating and fire hazards
5	March, 2010	Two iPod Nano music player overheating and catching fire, Japan	Caused by overheated lithium batteries
6	January, 2010	Two EV buses catch fire, Urumqi, China	Caused by overheated $LiFePO_4$ batteries
7	July, 2009	Cargo plane catch fire before fly to USA, Shenzhen, China	Caused by spontaneous combustion of lithium ion batteries
8	21 June, 2008	Laptop catch fire in a conference, fire burning 5 min, Japan	Caused by overheated battery
9	June, 2008	Honda HEV catch fire, Japan	Caused by overheated $LiFePO_4$ batteries
10	2006–now	Tens of thousands of mobile phone fires or explosions	Caused by short-circuit, overheating, etc.

Note: all the accident data are from the Internet.

3. Lithium ion battery fire accidents

A lot of fires and explosions have been reported throughout the world, Table 1 lists some of the reported lithium ion battery fires during the past years. It can be seen that the fires are caused by overheated both for the mobile phone battery and the EV batteries, that is the thermal runaways were triggered. The fires and explosions involving lithium ion batteries are rare in probability, occurring in anywhere from one in 1 million to one in 10 million batteries according to the best estimates. Still, these widely-publicized incidents have worried consumers and forced costly recalls of millions of batteries [10]. Some international computer companies announced large recalls of laptop batteries in the summer and October of 2006.

Lithium ion battery potential fire risk also threatens the transportation. At least nine fires involving lithium ion batteries have happened on airplanes or in cargo destined for planes since 2005, according to federal safety records reviewed by USA TODAY [11]. Numerous lithium ion battery explosions were reported in the worldwide on the internet, especially for the cell phones and laptops lithium ion battery as shown in Table 1.

It is commonly thought that the lithium ion battery fire and explosion is related to the flammability of the electrolyte, the rate of charge and/or discharge, and the engineering of the battery pack [5,12]. It can rupture, ignite, or explode when exposed to high temperature or short-circuiting. The adjacent cells may also then heat up and fail, in some cases, causing the entire battery to ignite or rupture [13].

The lessons from the accidents have told us that safety is a serious issue in lithium ion battery technology. Consequently, many approaches are being studied with the aim of reducing safety hazards. Unfortunately, all of them are expected to depress the specific energy [14]. Thus, the practical value of these approaches depends on whether an acceptable compromise between energy and safety can be achieved. Currently, the safer lithium ion batteries are mainly used in electric cars and other large-capacity battery applications, where safety issues are critical. The following sections review the main progress and in the lithium ion battery thermal runaway caused fire, and give some perspectives for the future.

4. Lithium ion battery thermal runaway mechanism

Thermal runaway is one of the failure modes in batteries. Many researches have been conducted to find the exact cause of this issue and how to prevent it [15]. Generally, thermal runaway occurs when an exothermic reaction goes out of control, that is the reaction rate increases due to an increase in temperature causing a further increase in temperature and hence a further increase in the reaction rate [16,17], which possibly resulting in an explosion. It is proposed that above 80 °C, thermal runaway can occur spontaneously as a result of fire or explosion [18]. For the lithium ion battery runaway, it is caused by the exothermic reactions between the electrolyte, anode and cathode, with the temperature and pressure increasing in the battery, the battery will rupture at last.

4.1. Theory analysis

The temperature of a lithium ion cell is determined by the heat balance between the amount of heat generated and that dissipated by the cell [12,19,20]. The heat generation follows the exponential function and the heat dissipation keeps the linear function [21]. When a cell is heated above a certain temperature (usually above 130–150 °C) [12,22,23], exothermic chemical reactions between the electrodes and electrolyte set in will raise its internal temperature. If the cell can dissipate this heat, its temperature will not rise abnormally. However, if the heat generated is more than what can be dissipated, the exothermic processes would proceed under adiabatic-like conditions and the cell's temperature will increase rapidly. The rising temperature will further accelerate the chemical reactions, rather than the desired galvanic reactions, causing even more heat to be produced, eventually resulting in thermal runaway [19,22].

An elegant way to visualize thermal runway reactions is in the plots often referred to as Semenov plots [24] in Fig. 2. The curved line 4 represents the heat generation due to an exothermic reaction (exponential function, assuming Arrhenius law) while the straight lines represent the heat removal which is a linear function (Newton's law of cooling) at different coolant temperatures. For the lithium ion battery, the curve 4 is the combined results of reactions occurred in the cell during the thermal runaway process, and the

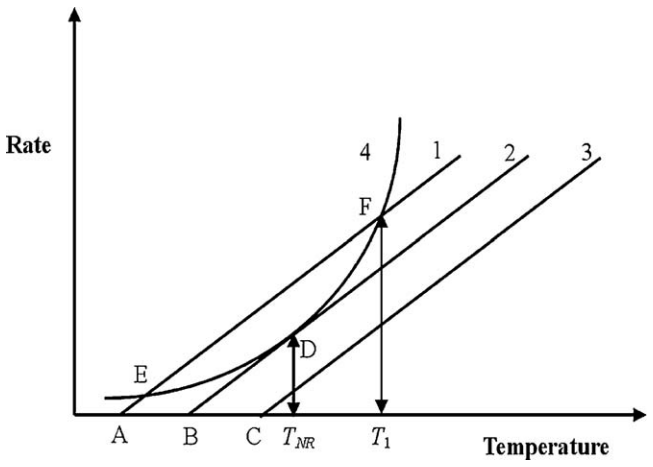

Fig. 2. Thermal diagraph of a reaction and heat loss from a vessel, at 3 ambient temperatures, A, B, and C. A can control the sample to temperature T_1, B is at the critical temperature T_{NR} and C cannot control the thermal runaway.
Adopted from Ref. [21].

reactions will be discussed in Section 4.2. The temperature of the coolant can be sufficiently low (case of line 1) or insufficiently, like in case 3 where thermal control is not possible under any circumstances. Line 1 has two points of intersection with line 4. Isothermal operation is possible in both points. The lower point E of intersection is a stable point. If temperature deviates upwards cooling power is higher than power generated by the reaction thus the system will return to the temperature of the stable point of operation. If temperature drops, as power generation is higher than power removal temperature will again return to that point. The second (higher point F of intersection), however, is an unstable one. If temperature drops it will go on dropping until it reaches the stable point, as power removal is higher than power generation, but if it deviates upwards the runaway is inevitable. Line 2 has one tangent point D with line 4, this point is a critical point, as heat removal is equal to heat generation, and thus, this critical equilibrium temperature is called the 'Temperature of No Return, T_{NR}'. The temperature B is called the self-accelerating decomposition temperature (SADT) [21]. The lithium ion battery can be regarded as a reaction system, in which heat is generated by the reactions between its compounds. And then, under different working and boundary conditions, when the battery temperature reaches to the T_{NR}, the thermal runaway will occur.

The above Semenov plots can explain the thermal runaway process simply and clearly, in which the heat generated by the reactions is the key issue as it dominates the thermal runaway processing. The heat generation is due to the chemical and electrochemical reactions and Joule heating inside the battery. The heat dissipation to the ambient is controlled by radiation and convection. The energy balance was proposed by many researchers. In general, the energy balance between the heat generation and heat dissipation is described as following [15,20,22,25–35]:

$$\frac{\partial(\rho C_p T)}{\partial t} = -\nabla(k\nabla T) + Q_{\text{ab-chem}} + Q_{\text{joul}} + Q_S + Q_P + Q_{ex} + \cdots \quad (1)$$

where ρ (g cm^{-3}) is the density, C_p (J g^{-1} K^{-1}) the heat capacity, T (K) is the temperature, t (s) is the time, k (W cm^{-1} K^{-1}) is the thermal conductivity. $Q_{\text{ab-chem}}$ is the abuse chemical reaction in the battery, and the detailed reactions will be discussed later. Q_{joul} is Joule heating in the battery, Q_S is the entropy change heat, Q_P is overpotential heat, and Q_{ex} is the heat exchange between the system and the ambient.

The reaction heat generation is the total result of all possible reactions when the battery is undergoing thermal runaway, mainly including solid electrolyte interface (SEI) decomposition, electrodes reaction with electrolyte, electrodes decomposition. For the individual reaction, the heat generation can be expressed as $Q_{\text{ab-chem}}$ [19]:

$$Q_{\text{ab-chem}} = \frac{dH}{dt} = \Delta H M^n A \exp\left(-\frac{E_a}{RT}\right) \quad (2)$$

where ΔH is the heat of reaction, M is the mass of reactant, n is the reaction order, A is pre-exponential factor, E_a is activation energy and R is gas constant. The total heat generation is the summarized values of all the reactions.

When a current flows through a device it induces Joule heating. In a lithium ion battery, the electrical resistance consists of the resistance of the positive and negative electrodes, electrolyte and separator. In each region, the current passes through different phases, hence Joule heating should be considered in all the phases. The Joule heating it the summarized value as [15]:

$$Q_{\text{joul}} = \sum_j |\phi_j \cdot i_j| \quad (3)$$

where ϕ_j is electric potential in phase j (V), i_j is current density in phase j (A cm^{-2}). Joule heating is always positive and contributes to a rise in temperature.

The heat Q_S by entropy change is described by the following equation [36]:

$$Q_S = IT\frac{\partial E_{\text{emf}}}{\partial T} \quad (4)$$

where T is battery temperature, I charge/discharge current (defined as positive during charge cycle), E_{emf} is cell potential for open-circuit. The reaction directions for charge and discharge cycles are opposite to each other, thus Q_S is endothermic during charge cycle and exothermic during discharge cycle.

When electric current flows through the cell, cell voltage V deviates from open-circuit potential V_0 due to electrochemical polarization. The energy loss by this polarization dissipates as heat. This overpotential heat Q_P is described as following equation [36]:

$$Q_P = I(V - V_0) = I^2 R\eta \quad (5)$$

where Q_P is exothermic during both charge and discharge cycles. When the difference between V and V_0 is expressed as $IR\eta$, Q_P can be determined from the overpotential resistance $R\eta$.

The radiation and the convection heat transfer are the main thermal exchanges between the cell surface and environments. When the battery temperature exceeds the ambient temperature, the convection starts to dissipate the thermal energy. When the battery is working at low temperatures, the effect of radiation can be neglected. But in high temperature batteries, radiation plays an important role and should be considered [15]. Convective and radiative heat flux out to ambient are evaluated in the following equations [15,22,31]:

$$Q_{\text{conv}} = hA(T_{\text{surf}} - T_{\text{amb}}) \quad (6)$$

$$Q_{\text{radi}} = \varepsilon\sigma A(T_{\text{surf}}^4 - T_{\text{amb}}^4) \quad (7)$$

where h is a convection heat transfer coefficient, A is the area of the case, ε is the emissivity of the cell surface and σ is the Stefan–Boltzmann constant. This equation shows that the radiation dissipation is a nonlinear function and is proportional to the fourth power of the temperature.

4.2. Basic reactions

The item $S_{\text{ab-chem}}$ involves several stages, and which are involved in the build up to thermal runaway and each one results in progressively more permanent damage to the cell. Normally, the battery undergoes the following reactions: SEI decomposition, reaction between the negative active material and electrolyte, reaction between the positive active material and electrolyte, electrolyte decomposition, and the reaction between the negative active and binder, etc. [22,23]. These reactions not react in an exact given order, some of them may be occur simultaneously.

The first stage is the breakdown of the thin passivating SEI layer on the anode, due to overheating or physical penetration. The SEI layer is mainly consist of stable (such as LiF, Li_2CO_3), and metastable components (such as polymers, $ROCO_2Li$, $(CH_2OCO_2Li)_2$ and ROLi) [9,23,37–41]. The metastable components can decompose exothermically at 90–120 °C as following [42].

$$(CH_2OCO_2Li)_2 \rightarrow Li_2CO_3 + C_2H_4 + CO_2 + \frac{1}{2}O_2 \quad (8)$$

The SEI layer decomposes at the relatively low temperature of 69 °C [39], and once this layer is breached the electrolyte will react with the carbon anode during the formation process but at a higher, uncontrolled, temperature. This is an exothermal reaction which drives the temperature up still further. The initial overheating may

be caused by excessive currents, overcharging or high external ambient temperature.

As the temperature builds up, heat from SEI decomposition reaction causes the reaction of intercalated lithium with the organic solvents used in the electrolyte releasing flammable hydrocarbon gases (ethane, methane and others) but no oxygen [23].

$$2Li + C_3H_4O_3\,(EC) \rightarrow Li_2CO_3 + C_2H_4 \quad (9)$$

$$2Li + C_4H_6O_3\,(PC) \rightarrow Li_2CO_3 + C_3H_6 \quad (10)$$

$$2Li + C_3H_6O_3\,(DMC) \rightarrow Li_2CO_3 + C_2H_6 \quad (11)$$

This typically starts at 100 °C but with some electrolytes it can be as low as 68 °C [39,43]. The gas generation due to the breakdown of the electrolyte causes pressure to build up inside the cell. Although the temperature increases to beyond the flashpoint of the gases released by the electrolyte the gases do not burn because there is no free oxygen in the cell to sustain a fire.

At around 130 °C the polymer separator melts [44,45], allowing the short circuits between the electrodes. Eventually heat from the electrolyte breakdown causes breakdown of the metal oxide cathode material releasing oxygen which enables burning of both the electrolyte and the gases inside the cell. Common used cathodes materials are $LiCoO_2$, $LiMn_2O_4$, $LiFePO_4$, $LiNiO_2$, and others. The charged positive active materials can disproportionate at elevated temperatures, $LiCoO_2$ as an example, as follows [46–50]:

$$Li_xCoO_2 \rightarrow xLiCoO_2 + \frac{1}{3}(1-x)Co_3O_4 + \frac{1}{3}(1-x)O_2 \quad (12)$$

$$Co_3O_4 \rightarrow 3CoO + 0.5O_2 \qquad CoO \rightarrow Co + 0.5O_2 \quad (13)$$

The oxygen released might react with solvent as follows, EC as an example [23]:

$$2.5O_2 + C_3H_4O_3\,(EC) \rightarrow 3CO_2 + 2H_2O \quad (14)$$

The breakdown of the cathode is also highly exothermic sending the temperature and pressure even higher. The exothermic heat based on cathode weight is about $1000\,J\,g^{-1}$, which is larger than the exothermic heat of electrolyte [50]. For the 1.0 M $LiPF_6$/EC + DEC-$Li_{0.5}CoO_2$ system, it starts to release heat at 128 °C and reaches to exothermic peak temperatures at 196 °C, 205 °C and 230 °C with a total heat generation of $-1052.6\,J\,g^{-1}$ [46]. The released oxygen and heat provide the required conditions for combustion in the cell.

Carbon remains the pre-eminent anode material for lithium-ion batteries because of its good performance. After the breakdown of SEI layer formed on anode, the lithiated anode material decomposes again. Actually it keeps releasing heat after the SEI decomposition, and reaches to the second exothermic peak about 210 °C with the presence of electrolyte [39]. The total heat generation can reaches $2000 \pm 300\,J\,g^{-1}$, which is dangerous for the battery. There is a small CO_2 evolution centered at 228 °C and POF_3 evolution between 200 °C and 240 °C [38,51]. It is contributed by the fact that the metallic lithium reacts with EC to produce carbon dioxide and dilithio butylene dialkoxide; the PF_5 decomposed from $LiPF_6$ reacts with dilithio butylene dialkoxide to produce POF_3 as following [51]:

$$2Li + 2EC \rightarrow Li\text{–}O\text{–}(CH_2)_4\text{–}O\text{–}Li + 2CO_2 \quad (15)$$

$$LiPF_6 \rightarrow LiF + PF_5 \quad (16)$$

$$Li\text{–}O\text{–}(CH_2)_4\text{–}O\text{–}Li + PF_5 \rightarrow Li\text{–}O\text{–}(CH_2)_4\text{–}F + 2LiF + POF_3 \quad (17)$$

The common electrolytes are cyclic alkyl carbonate and chain alkyl carbonate solution, with lithium hexafluorophosphate ($LiPF_6$) as the solute. Since the alkyl carbonate solvents including propylene carbonate (PC), ethylmethyl carbonate (EMC), EC, DEC and dimethyl carbonate (DMC) are flammable, they may cause fire or explosion hazard under the abuse conditions of battery operation. The electrolyte not only reacts with the electrodes, but also decomposes itself at elevated temperature. Fourier transform infrared reflectance (FTIR), nuclear magnetic resonance (NMR), mass spectroscopy (MS) and thermal analysis have proved that it decomposes at about 200–300 °C and produces CH_3CH_2F, FCH_2CH_2Y (Y is OH, F, etc.) CO_2, etc. [43,52–54].

$$C_2H_5OCOOC_2H_5 + PF_5 \rightarrow C_2H_5OCOOPF_4 + HF + C_2H_4 \quad (18)$$

$$C_2H_4 + HF \rightarrow C_2H_5F \quad (19)$$

$$C_2H_5OCOOPF_4 \rightarrow PF_3O + CO_2 + C_2H_4 + HF \quad (20)$$

$$C_2H_5OCOOCPF_4 \rightarrow PF_3O + CO_2 + C_2H_5F \quad (21)$$

$$C_2H_5OCOOCPF_4 + HF \rightarrow PF_4OH + CO_2 + C_2H_5F \quad (22)$$

By this time the pressure is also extremely high. The cells are normally fitted with a safety vent which allows the controlled release of the gases to relieve the internal pressure in the cell avoiding the possibility of an uncontrolled rupture of the cell. Once the hot gases are released to the atmosphere they can of course burn in the air.

There are some other reactions in the lithium ion battery, such as, reactions between the fluorinated binder and the electrode materials. Other than providing sufficient mechanical strength and maintaining integrity of the electrodes, the binder also affects the thermal stability of electrode under elevated temperature.

Markevich et al. [55] reported that the presence of PVDF binder can increase the $LiCoO_2$ reactivity (probably at contact points). The authors suggested that PVDF forms H-bonds, which increases the local concentration of acidic species close to the surface of the $LiCoO_2$ particles, which enhances the $LiCoO_2$ decomposition. Furthermore, for the $LiCoO_2$ electrodes containing PVDF, the main surface reaction relates to $Co^{III} \rightarrow Co^{II}$ reduction and the major decomposition product is Co_3O_4, accompanied by the oxidation of some solution species [56]:

$$4LiCo^{III}O_2 \rightarrow Co^{IV}O_2 + Co^{II}Co^{III}O_4 + 2Li_2O \xrightarrow{4HF} 4LiF + 2H_2O \quad (23)$$

For the PVDF–Li_xC_6 reactions, they are strongly affected by the degree of lithiation of the graphite since they occur only when the carbon electrode is lithiated [57]. In the presence of electrolyte as the acidic medium, PVDF was dehydrofluorinated according to the following equation [58]:

$$\text{–}CH_2\text{–}CF_2 \rightarrow \xrightarrow{base} \text{–}CH = CF\text{–} + HF \quad (24)$$

Then a possible reaction between the binder and the Li_xC_6 electrode is as follows [57]:

$$\text{–}CH_2\text{–}CF_2 + Li \rightarrow LiF + \text{–}CH = CF\text{–} + 0.5H_2 \quad (25)$$

These reactions occur when the temperature is higher than 260 °C and the heat for the reaction of $Li_{0.85}C_6$ with PVDF is $1220\,J\,g^{-1}$.

All the above reactions contribute heat and pressure in the cell and in return speed up the reactions. It should be noted that the reactions are not one after one in an exact order, they are influencing each other and show some chaos. Therefore, it is difficult to judge the exact reactions and their sequence during the thermal runaway occurring.

4.3. Thermal models

In battery applications, a number of cells are packed together in various configurations (parallel and/or series connected) to form a module. Several modules are then combined in series or parallel to provide the required voltage and capacity for a specific application as shown in Fig. 3. Therefore, the battery thermal models should be designed for the specified configuration. Many kinds of

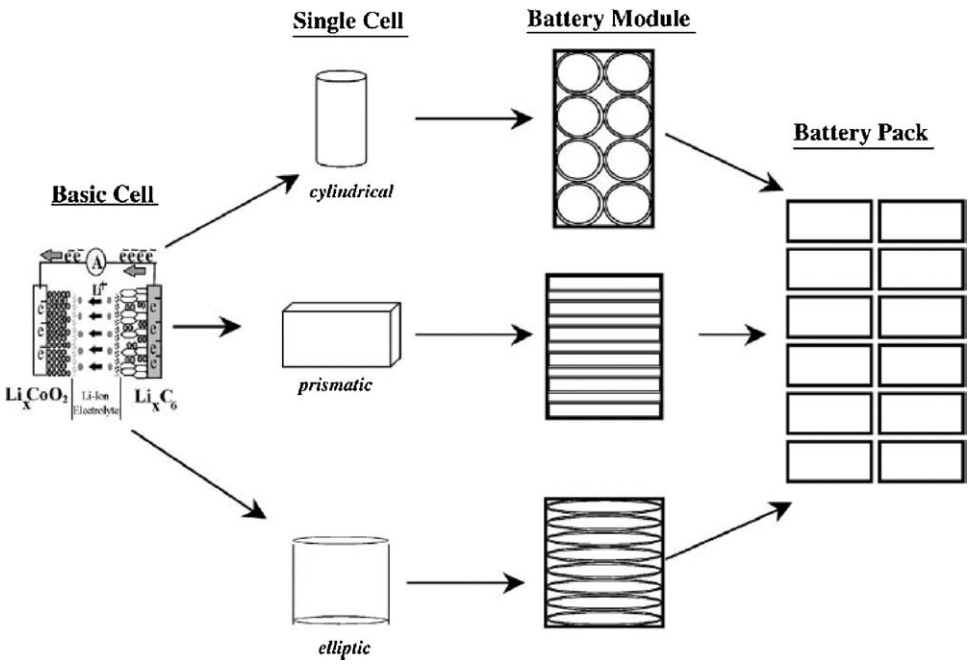

Fig. 3. Schematics of the battery pack design with different cell configurations.
Adopted from Ref. [209].

the corresponding thermal models have been introduced for the lithium ion batteries in the past 15 years. Doughty et al. [28] proposed two general approaches that can be used to build thermal abuse models of lithium-ion cells. They are the calorimetry-based approach [27,59] and the chemical reaction approach, respectively. The calorimetry approach is based on a simplified model of cell construction. It uses measured thermal properties of cell components, which are characterized by reaction rate equations using Arrhenius thermal activation energy terms. These properties are determined as a function of state-of-charge (SOC) and can include anode/electrolyte, cathode/electrolyte, and electrolyte decomposition reactions. Cycle/ageing history can be accounted for from measurements on aged cells. Other data required are accurate determination of cell component heat capacities and thermal conductivities along with the cell dimensions. Another approach to construct the thermal model is based on the chemical reactions, which requires the identification of the chemical reactions responsible for each of the dominant thermal events. Furthermore, the reaction rates and activation energies should be determined for each of these reactions. A model is also needed for predicting the reaction product species on the electrodes, which will serve as source terms contributing to the heat producing reactions. Finally, the chemical terms must be combined with details of the cell construction in order to simulate thermal behavior for the overall cell. This requires knowledge of bulk thermal properties of the cell materials [16,28,60,61]. In general, the models can be classified to three types in dimension, one-dimensional, two dimensional and three dimensional models. It also can be classified in its functions, to simulate the oven test, short circuit, and so on.

One dimensional model assumes simplified cell design and mode of operation with isothermal, constant current, lumped thermophysical properties, and constant heat generation rates. Al Hallaj et al. [62] presented a simplified one-dimensional thermal model with lumped parameters to simulate the temperature profiles inside lithium ion cells. The energy balance in the cell is described in spherical coordinates by following equation [62]:

$$\frac{\partial^2 T}{\partial r^2} + \frac{1}{r}\frac{\partial T}{\partial r} + \frac{q}{k_{\text{cell}}} = \frac{1}{\alpha}\frac{\partial T}{\partial t} \tag{26}$$

Pals and Newman [63,64] neglected the effect of temperature change on battery performance and presented a one-dimensional model for predicting the thermal behavior of lithium polymer batteries for a single cell and a cell stack. The model can be used to simulate a wide range of polymeric separator materials, lithium salts, and composite insertion electrodes. A lumped-parameter thermal model of a cylindrical $LiFePO_4$/graphite lithium-ion battery was developed [32]. This model allows for simulating the internal temperature directly from the measured current and voltage of the battery. Later the thermal model was extended to the HEV battery pack by Smith [65], and resulted that the pack generates heat at a 320 W rate on a US06 driving cycle at 25 °C, with more heat generated at lower temperatures. However, the reaction and electronic phase ohmic heats are negligible. One-dimensional model only can predict the temperature profile along one dimension. The one-dimensional model only was used at the early stage in the lithium ion battery developments, and no more effort is on it now.

The two-dimensional model considers two dimensions in radius and azimuthal coordinates for the cylindrical cell, in width and length directions for the prismatic battery. A lot of two-dimensional models were proposed to model the battery thermal response under various state of charge, discharge, and statics situation. The heat flow inside a battery is exceedingly dominated by conduction in radial and angular directions, which is given in spherical coordinates by the following equation, and the density, heat capacity, and thermal conductivity vary with location.

$$\rho C_p \frac{\partial T}{\partial t} = \frac{1}{r}\frac{\partial}{\partial r}\left(k_r r \frac{\partial T}{\partial r}\right) + \frac{1}{r^2}\frac{\partial}{\partial \phi}\left(k\phi \frac{\partial T}{\partial \phi}\right) + q \tag{27}$$

The above equation is the basic thermal model to predict the temperature distribution. Further improvements were made on the battery state, such as, the anode (carbon) decomposition reaction were considered to predict the temperature of a lithium-ion cell during medium- and high-rate discharge conditions [66–68]. It is good that the transport of lithium ions across the cell and within the solid-phase particles was considered and it is assumed to be spherical. The 2D model also can be expressed in Archimedean spiral format, this method was used by Chen et al. [69]. This kind of

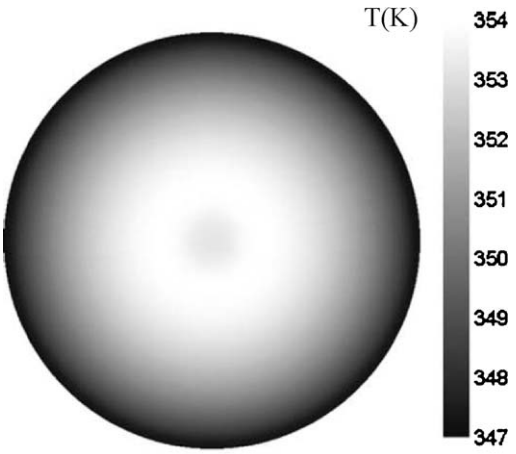

Fig. 4. A two-dimensional temperature distribution of battery with spiral geometry. Adopted from Ref. [69].

two-dimensional thermal model deals properly with a numerical solution of high precision for the complicated spiral geometry [69]. The temperature distribution of a 10 Ah lithium battery at the end of 3 C discharge was obtained and shown in Fig. 4 [69]. The temperature at the angular direction is fairly uniform and heat is mainly transferred along the radial direction. The maximum temperature is located on the a circular region neighboring the hollow core.

The two-dimensional model in Cartesian coordinates was proposed for the prismatic battery as following [70]:

$$\rho C_p \frac{\partial T}{\partial t} = k_X \frac{\partial^2 T}{\partial x^2} + k_Y \frac{\partial^2 T}{\partial y^2} + q \tag{28}$$

where T is the temperature, C_p is heat capacity, x is the direction perpendicular to the cells, and y is the direction parallel to the cells. The diffusion coefficient of lithium ions, ionic conductivity of lithium ions, transference number of lithium ions, were characterized for the thermal behavior of the lithium polymer system [70]. The reversible, irreversible, and ohmic heats in the matrix and solution phases were considered in another two-dimensional thermal-electrochemical model developed by Srinivasan and Wang [71]. In their model, the heat generation rate is determined by experimental data, instead of an electrochemical model. The two-dimensional anisotropic cylindrical coordinate model with linear triangular finite elements was used to simulate the steady-state temperature distribution within the cell. The effects of material and design modifications on the temperature distribution of lithium ion cells were considered and simulated numerically [72]. The two-dimensional model for thin-film batteries were proposed by Baker and Verbrugge [73]. In their model, the cell energy, power, and thermal characteristics are constructed to determine both the position and magnitude of the maximum temperature during rapid charge and discharge. The two-dimensional model is better than one-dimensional model, as it can display a basic temperature distribution. The process in lithium ion battery to overheating is quite complicated, which couples the electrochemical process, chemical reactions, heat generation and heat transfer. In this aspect, two-dimensional model is not enough to simulate the real case of the battery thermal runaway.

The three-dimensional model is more powerful and flexible in simulating the thermal performance of batteries with different parameters and assisting the design of thermal management systems. Chen and Evans [25,74] developed three dimensional models to study the thermal behavior of lithium polymer batteries and lithium ion batteries. They assumed that the heat generation rate is uniform throughout the cell, and actually, it is a simple way to deal with the heat generation distributions, and then, they gave the energy conservation equation as follows [74]:

$$\rho C_p \frac{\partial T}{\partial t} = k_X \frac{\partial^2 T}{\partial x^2} + k_Y \frac{\partial^2 T}{\partial y^2} + k_Z \frac{\partial^2 T}{\partial z^2} + q \tag{29}$$

The models precisely consider the layered-structure of the cell stacks, the case of a battery pack, and the gap between both elements to achieve a comprehensive analysis. Based on this model, some important phenomena such as the asymmetric temperature profile and the anomaly of temperature distribution on the surface can be simulated precisely [31]. The three-dimensional thermal abuse model on lithium-ion batteries was developed by Guo et al. [75]. The model coupled with electrochemical reaction and thermal response to study in detail the temperature field distribution and evolution inside cell. It also considers the geometrical features to simulate oven test, which are significant in larger cells for electric vehicle application.

Recently, more efforts were focused on the electrochemical thermal coupled models [35,76–81], and most of the models are one dimensional ones. Guo et al. [77] extended the single-particle model presented by Santhanagopalan et al. [82] to an electrochemical thermal model which including an energy balance. Cai and White [83] extended the existing lithium ion battery model in multiphysics software (COMSOL) to include the thermal effects. This kind of model considered the electrochemical process under normal and abuse conditions of the battery, such as discharge, external shorts, short-circuit [35,76,78,79]. The electrochemical model is shown in Fig. 5 in a sketch map. The active material within each electrode is approximated to spherical particles arranged along the thickness of the electrode. The electrode is treated as a superimposed continuum of the solid phase and the electrolyte. Diffusion and kinetic parameters are held constant and thermal effects are assumed to be negligible. The material balance for the lithium ions in an active solid material particle is governed by Fick's second law in spherical coordinates [77,83,84]:

$$\frac{\partial c_{s,i}}{\partial t} = D_{s,i} \frac{1}{r^2} \frac{\partial}{\partial r} \left(r^2 \frac{\partial c_{s,i}}{\partial r} \right) \tag{30}$$

Santhanagopalan et al. [79] developed an electrochemical thermal model to study the internal short-circuit behavior of a lithium ion cell. Several short-circuit scenarios possible in a lithium ion cell were simulated and the influence of parameters like the SOC and initial temperature of the cell was studied. They used an unscented filtering algorithm to estimate the SOC for high power lithium ion cells [84]. Cai and White [80,83] proposed an orthogonal decomposition method to develop an efficient, reduced order electrochemical-thermal model for a lithium-ion cell. The model predictions indicate that the discharge time or percent of capacity removed from the cell at an end of discharge voltage depends on the rate of the discharge and heat transfer rate away from the cell. Fang et al. [81] developed the electrochemical–thermal coupled model to predict performance of a lithium-ion cell as well as its individual electrodes at various operating temperatures. The predictive ability of the individual electrode behavior is very useful to address important issues related to electrode degradation and subzero performance of automotive lithium ion batteries. In the EV or other larger lithium ion battery driving equipments, at the sudden onset of the equipments, it need a larger transit discharge current, which will generate great heat. The heat generated at this process is dangerous to trigger the thermal runaway reactions in the battery, the existing thermal models are not considered the extreme conditions. The other extreme working conditions of battery should also be considered in the simulation of the real case thermal runaway of a lithium ion battery. Furthermore, to predict the onset temperature of thermal runaway accurately is another challenge.

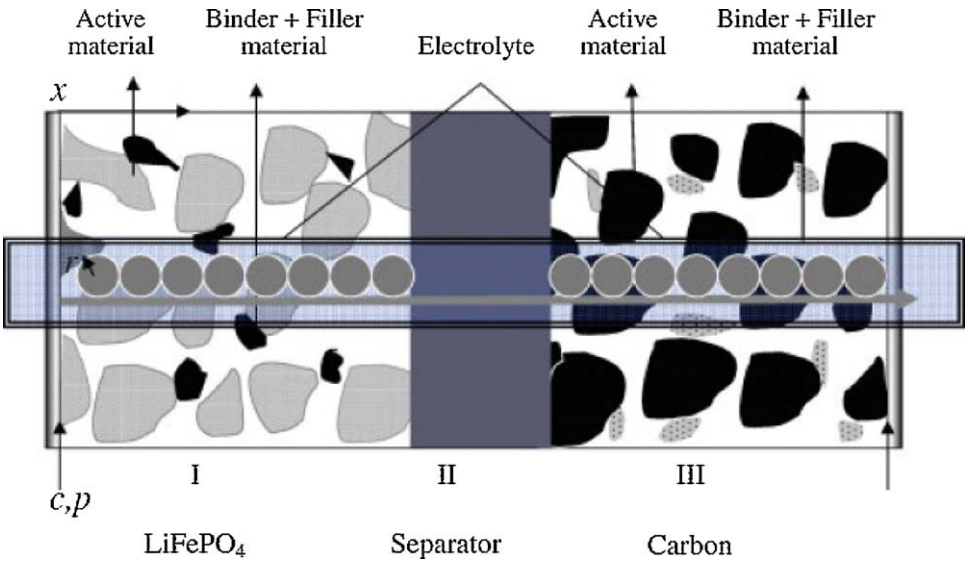

Fig. 5. Schematic of the electrochemical model.

Adopted from Ref. [84].

The thermal runaway is comprehensive results of different process, which includes the electrochemical, materials activity and interactions, discharging rate, packing and so on. Every part is a complex system, and they are influenced by each other. The first step is to discover the mechanism, and then to model it. At present, it is not a easy work to model every process, combine them together and make it working well.

The above models are developed for single lithium ion cell, in most cases, the cells are packed together for use. Therefore, to develop the thermal–electrical model for lithium ion cell modules is necessary for the application of battery. The first three-dimensional model for large scale lithium-polymer battery modules was proposed by Verbrugge [85] to treat simultaneously the temperature and current distributions. His calculations illustrate the nonlinear dependence of power output on system temperature is possible lead to thermal runaway. Smith et al. [78] developed a thermal–electrical model for module with 16 cells in parallel. Another nine-cell stacking model is proposed and analyzed for its effect for different cooling methods [86]. Furthermore, the battery pack dynamic models for electrical-drive vehicles or for virtual-prototyping of portable battery-powered systems were developed [87–89]. The dynamic model structure adopted is based on an equivalent circuit model whose parameters are scheduled on the state-of-charge, temperature, and current direction. Coupled with the Battery Design Studio, Spotnitz et al. [16] developed the battery pack thermal behavior model to predict single cell effect on the others. Thermal runaway of the pack is more likely to be induced by thermal runaway of a single cell when that cell is in good contact with other cells and is close to the pack wall [16].

Oven exposure testing in a standard benchmark that lithium ion cells must pass in order to be approved for sale by regulating bodies. The model for oven exposure testing has been developed by Hatchard et al. [27], The model can predict the response of new cell sizes and electrode materials to oven exposure testing without actually producing any cells. The catastrophe theory was used in lithium ion battery thermal runaway, and it was found that the thermal runaway of lithium ion battery is a swallowtail catastrophe [19]. This is interesting to plot the thermal runaway zones as shown in Fig. 6 [19], however, the physical meanings of the parameters in the swallowtail catastrophe model need be explained further. Other related models are similar for a given battery or battery packs [20,25–28,30,31,36,62,90,91].

4.4. Simulation works

In recent years, finite volume method (FVM) and finite element method (FEM) were used to simulate the temperature distribution of lithium ion battery during charging/discharging based on the thermal models. Furthermore, the researches on battery pack thermal simulation also were conducted, and the one cell thermal runaway effect on other cells was investigated.

The finite volume method is a method for representing and evaluating partial differential equations (PDE) in the form of algebraic equations. Similar to the finite difference method or finite element method, values are calculated at discrete places on a meshed geometry. This method was used to simulate the thermal behavior of lithium ion battery. One-dimensional model for oven exposure testing was first developed by Hatchard et al. [27]. Then it was extended to three dimensions by Kim et al. [22]. The model is based on finite volume method to conduct three-dimensional thermal abuse simulations for lithium ion batteries. The three-dimensional model captures the shapes and dimensions of cell components and the spatial distributions of materials and temperatures, and was used to simulate oven tests, and to determine how a local hot spot can propagate through the cell. The model results show that smaller cells reject heat faster than larger cells; this may prevent them from going into thermal runaway under identical abuse conditions. In simulations of local hot spots inside a large cylindrical cell, the three-dimensional model predicts that the reactions initially propagate in the azimuthal and longitudinal directions to form a hollow cylinder-shaped reaction zone. Fig. 7 is the simulated results, and the battery undergoing thermal runaway at 64 min a 155 °C under their oven test conditions. Another finite volume approach was conducted by Freitas et al. [92]. based on the commercial computational fluid dynamics (CFD) software Phoenics, the related 2D transport equations were solved, giving the time-dependent temperature profiles. It is found the generation of electrical current occurs immediately after the thermite burning. The FVM also was used to solve the coupled electrochemical-thermal model by Zhang [35]. Three types of heat generation sources including the ohmic heat, the active polarization heat and the reaction heat were quantitatively analyzed for the battery discharge process. The ohmic heat is found to be the largest contribution with around 54% in the total heat generation. About 30% of the total heat generation in average is ascribed to the electrochemical reaction. The active polarization

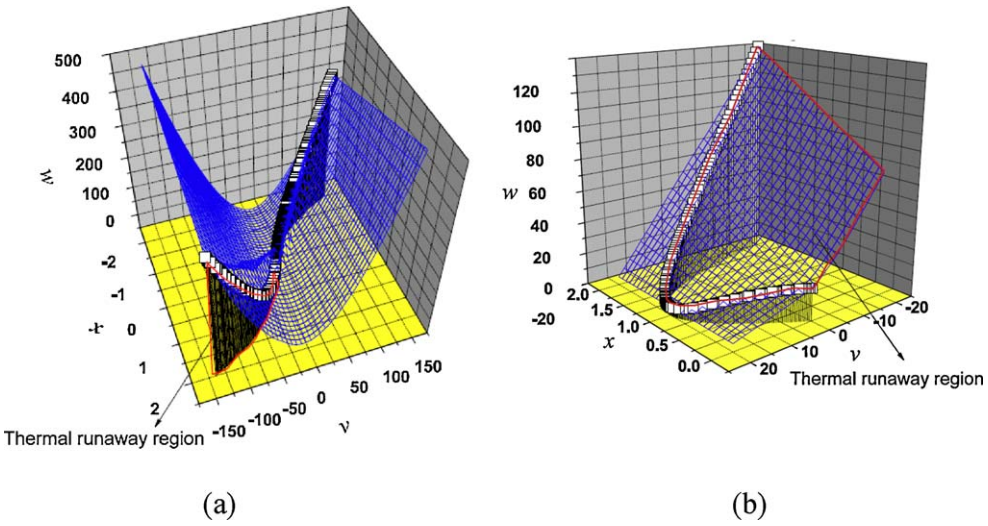

Fig. 6. Thermal runaway zones of lithium ion battery based on the bifurcation set of swallowtail catastrophe (a) at $u \geq 0$ ($u = 10$); (b) at $x > 0$ and $u < 0$ ($u = -10$). u, v and w are control parameters used in catastrophe model.
Adopted from Ref. [19].

contributes the least comparing to the ohmic heat and reactions heat.

The finite element method is a numerical technique for finding approximate solutions of PDE as well as of integral equations. The solution approach is based either on eliminating the differential equation completely, or rendering the PDE into an approximating system of ordinary differential equations, which are then numerically integrated using standard techniques such as Euler's method, Runge–Kutta, etc. The FEM was also used to develop the three-dimensional thermal abuse model on lithium-ion batteries by Guo et al. [75]. The model coupled with electrochemical reaction and thermal response to study in detail the temperature field distribution and evolution inside cell. Similar with Kim's finite volume result, the battery undergoes thermal runaway at 60 min in the 155 °C oven, which agrees well with Kim's result. The thermal behavior of a lithium-ion battery during charge was presented later by Kim [68,93,94], and the temperature distributions were obtained from the models. The transient and thermo-electric finite element analysis (FEA) of cylindrical lithium ion battery was presented in cylindrical coordinate [76]. This model provides the thermal behavior of lithium ion battery during discharge cycle. The mathematical model solves conservation of energy considering heat generations due to both joule heating and entropy change. The contribution of heat source due to joule heating was significant at a high discharge rate, whereas that due to entropy change was dominant at a low discharge rate.

The finite element software LS-DYNA and ABAQUS were used to analyse the jelly roll while charging and impact test, respectively. Except the temperature distribution, the stress distribution was also plotted, and Fig. 8 is the typical Von Mises stress [95]. The simulation results provided insights into the extent to which cylindrical cells can endure abnormal conditions. Furthermore, the CFD, ANSYS FLUENT, was used for the thermal management of traction battery systems of electrical-drive vehicles [89].

In the above simulations, the chemical reactions are simplified or even not considered, which is not sufficient to predict the real situation in the battery. The battery is simply regarded as homogenous material, and electrolyte, anode and cathode are combined to one material. Further researches should consider the reactions and mesh the electrodes separately.

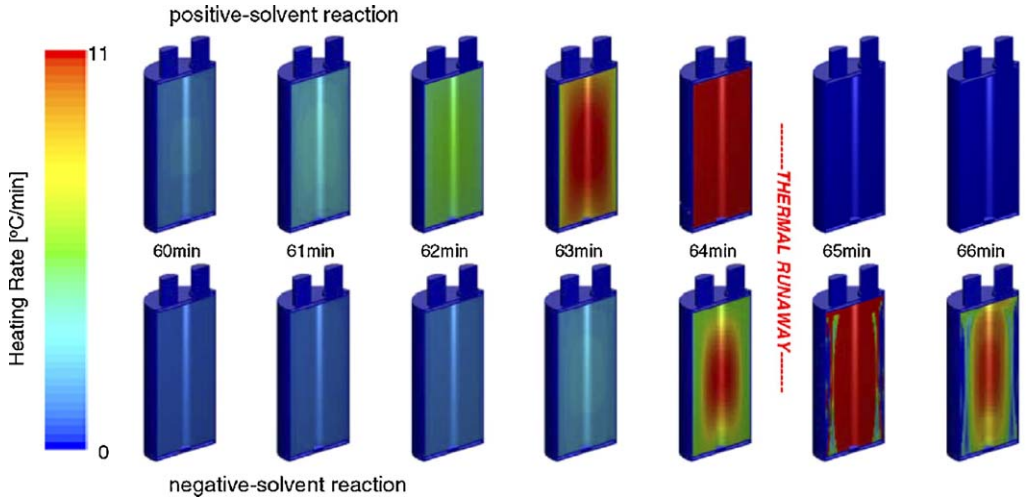

Fig. 7. Simulated sequence of component heat generation contours for a D50H90 cell in a 155 °C oven test using three-dimensional model.
Adopted from Ref. [22].

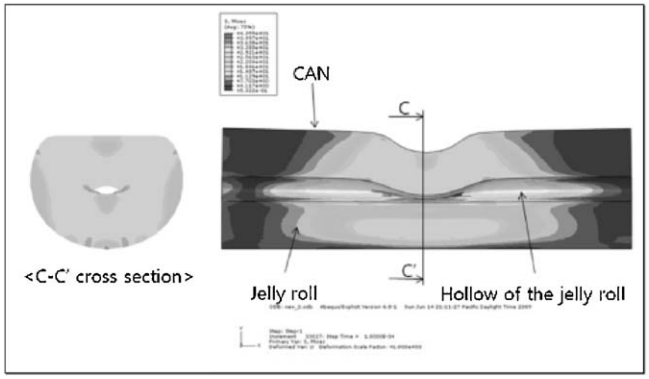

Fig. 8. Von Mises stress contour for impact test.
Adopted from Ref. [95].

4.5. Experimental works

Based on the materials thermal behaviors, some abuse experiments were conducted for kinds of lithium ion batteries [61]. The widely used methods to evaluate the abuse tolerance of lithium ion battery are oven test, short-circuit, overcharge, nail, crush test and so on [23,96–98].

(1) *Oven test*: This test simply involves exposing the battery, at some initial temperature, to a higher temperature. For consumer batteries, an oven temperature of 150 °C is used. This method is used to verify the safety quality of cell and compare with related thermal model of lithium ion battery [59,75]. The NEC Moli energy 18650 cells containing $LiMn_2O_4$ cathode [59] and $LiFePO_4$/graphite cells were verified [75].
(2) *Short-circuit*: A low resistance (<5 mΩ) is connected across the terminals of the battery. In this test, current flows through the battery generating heat. The battery is heated internally due to current flow, but the external circuit can dissipate heat also. Orendorff et al. [99] described the development of an experimental technique to trigger internal short circuits in lithium-ion cells. The technique involves the introduction of a low melting point metal foil during the construction of a cell that causes an internal short after a phase change. Internal shorts can be triggered in 2032 coin cells and 18650 cells using this approach. Under short-circuit conditions the cells remain hermetically sealed, and reach an internal temperature of 132 °C for $LiCoO_2$/graphite lithium ion battery [100]. Santhanagopalan et al. [79] found the cells with higher states of charge progressively show an exponential rise in the rate of increment of the average cell temperature, even higher to 700 °C for the fully charged battery in their simulations.
(3) *Overcharge test*: Current is forced through the cell up to some limiting voltage. Heat is generated by electrochemical reactions and by current flowing through the cell. The rate of charge was found to be an important parameter, as cells overcharged at low charge rates remained hermetic while high charge rates (C/2 and above) resulted in cell rupture. The internal temperature of the cells monitored during overcharge was found to be as high as 195 ± 5 °C, which was 93 °C higher than the external skin temperature of the cell [100,101]. This causes a cell charged at the 1 C rate to lose cycle ability and a cell charged at the 3 C rate to undergo explosion [102]. These overcharge and high discharge currents promote joule heat within the cells and leads to decomposition and release of oxygen from the delithiated Li_xCoO_2 and combustion of carbonaceous materials. The reactions between overcharged anode (deposited lithium) and electrolyte causes the thermal runaway with the cell rupturing [103,104], the oxygen, generated from the reactions, plays a key role to thermal runaway for the lithium ion battery under overcharged test [105].
(4) *Nail*: A nail is forced through the battery at a prescribed rate (such as 8 cm s^{-1}). Heat is generated by current flowing through the cell, and by current flowing through the nail. Initially the nail is positioned outside of the battery wall and, when the test begins, is forced through the battery wall and into the battery at a constant speed. As the nail moves forward, forming direct shorts between adjacent electrode pairs, the current flowing through the nail itself decreases. In nail penetration and impact tests, a high discharge current passing through the cells gives rise to thermal runaway [97,102].
(5) *Crush test*: A bar is used to press down on the battery until a short-circuit initiates. The battery heats up due to over potential losses at the electrodes and activates the negative/solvent reaction. This further heats the battery, activating the positive decomposition reaction and causing thermal runaway [23].

Furthermore, the combustion tests were performed on commercial pouch cells by means of the Fire Propagation Apparatus [106]. The mass loss and combustion gas production (HF, CO, NO, SO_2 and HCl) can be obtained online, which can deduce the rate of heat release, heat of combustion and the mass of burnt products from the combustion tests. This test is helpful in evaluating the fire risk for EV and HEV used lithium ion batteries.

Some codes and standards have be developed by several organizations, such as the hazardous materials transport regulations developed by the United Nations (UN) (UN 38.3.4), Code of Federal Regulations (CFR) (49 CFR), the consumer electronics safety standards developed by UL(UL 1642 and UL 2054) and, more recently by the Institute of Electrical and Electronics Engineers (IEEE) (IEEE 1725 and IEEE 1625), and the International Electrotechnical Commission (IEC) (CEI/IEC 62133 and IEC 62281). These standards continue to define safety performance for lithium ion cells. A number of additional standards have recently been adopted or developed in Japan, China, or Korea. Currently, the automotive industry is in the process of drafting new standards or revising existing standards for application to lithium-ion batteries [107]. The detailed regulations can be found in the above mentioned codes and standards.

5. Fire prevention measures for lithium ion battery

Lithium ion battery fire and explosion are triggered by the thermal runaway reactions inside the cell. The design for battery safety can be focused on the two methods, that is, inherent safety method and safety device.

5.1. Inherent safety methods

Safety issue of a battery starts from electrode materials and electrolyte to cell design, and the thermal runaway is a very complicated process involving chemistry, material science and engineering. The activity of the materials is the origin of the battery safety issue, SEI decomposition, the electrolyte reacting with cathode and anode and so on are releasing heat and contributing heat for thermal runaway. Therefore, to suppress the activity of the materials is the basic way to improve the battery safety. Although the different electrode materials, electrolytes and cell types show different thermal runaway behaviors, the thermal runaway mechanisms are similar, which are undergoing the heat accumulating process till the temperature of no return as stated in Section 4.1. As there are a lot of materials that can be used in the battery, and new materials are under developing, the detailed thermal runaway

behavior also is to be investigated. Therefore, the thermal runaway behavior for different materials are not fully compared here instead of the general idea to improve the safety of lithium ion battery.

5.1.1. Cathode materials

Cathode materials mainly include $LiCoO_2$, $LiNiO_2$, $LiMn_2O_4$, $LiFePO_4$ and so on. Modification by coating is an important method to achieve improved thermal stability. When the surface of cathode materials including $LiCoO_2$, $LiNiO_2$, $LiMn_2O_4$ and $LiMnO_2$ is coated with oxides such as MgO, Al_2O_3, SiO_2, TiO_2, ZnO, SnO_2, ZrO_2, and other materials, the coatings prevent the direct contact with the electrolyte solution, suppress phase transition, improve the structural stability, and decrease the disorder of cations in crystal sites. As a result, side reactions and heat generation during cycling are decreased [108–116]. Ternary material and $LiFePO_4$ are thought as the promising cathode materials of the next generation of large scale lithium ion battery for EV or HEV, because of their low price and "good safety", compared with conventional cathode materials (e.g. $LiCoO_2$) [117,118]. However, the fact of the bus fire caused by EV battery with $LiFePO_4$ as cathode materials exemplified that the safety is still potentially a major problem. Furthermore, their volumetric energy density and low temperature performance need to be solved [119,120]. Olivine-type $LiMnPO_4$ as cathodes deliver a flat voltage, excellent cycling stability and low entropy change throughout the state of charge, however, the charged $LiMnPO_4$ shows poor thermal stability [121,122]. Recently, a novel temperature-sensitive cathode material, $LiCoO_2$@P3DT was reported by Xia et al. [123]. This material has function of protect itself from thermal runaway at elevated temperature of 110 °C, which is good way to avoid the thermal runaway.

5.1.2. Anode materials

The thermal decomposition of the SEI is the most easily triggered chemical reaction in lithium ion cells and plays a critical role in determining the battery safety [124]. Therefore, to improve the thermal stability SEI is a critical way to enhance the safety of the anode. The SEI can be modified by mild oxidation, deposition of metals and metal oxides, coating with polymers and other kinds of carbons. Through these modifications, the surface structures of the graphitic carbon anodes are improved, which include [125]: (1) smoothing the active edge surfaces by removing some reactive sites and/or defects on the graphite surface, (2) forming a dense oxide layer on the graphite surface, and (3) covering active edge structures on the graphite surface. As a result, the direct contact of graphite with the electrolyte solution is prevented, its surface reactivity with electrolytes, the decomposition of electrolytes, the co-intercalation of the solvated lithium ions and the charge-transfer resistance are decreased, and the movement of graphene sheets is inhibited [125–130]. Great breakthrough were made using chemical activation of exfoliated graphite oxide to synthesize porous carbon, with a Brunauer–Emmett–Teller surface area of up to 3100 $m^2\ g^{-1}$, a high electrical conductivity, and a low oxygen and hydrogen content [131]. It is interesting that a natural polysaccharide extracted from brown algae was developed, which yields a stable battery anode possessing reversible capacity 8 times higher than that of the state of the art graphitic anodes [132]. However, the thermal stability of these materials and their compatibility are unknown and need to be investigated further.

5.1.3. Electrolyte

According to their functions, Zhang divided the additives into these categories [133]: (1) SEI forming improver, (2) cathode protection agent, (3) $LiPF_6$ salt stabilizer, (4) safety protection agent, (5) Li deposition improver, and (6) other agents such as solvation enhancer, aluminum corrosion inhibitor, and wetting agent.

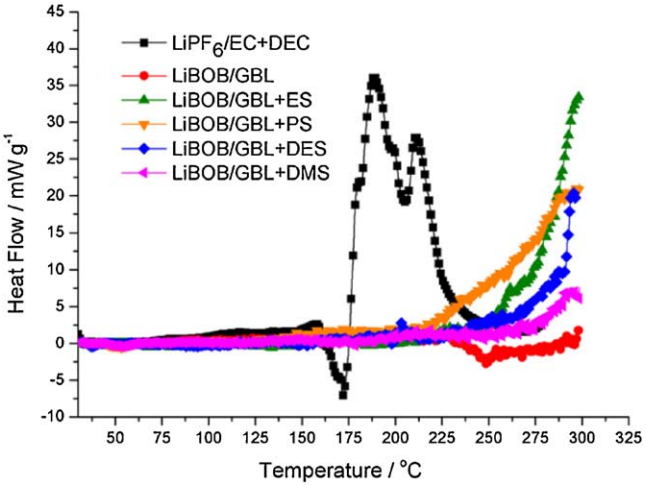

Fig. 9. Improved thermal stability of electrolyte using LiBOB/GBL series. Adopted from Ref. [168].

Here we just discuss the safety protection agent, which includes flame/fire retardant (FR) additive and overcharge additive.

5.1.4. Flame retardant additive

An ideal FR should be more efficient in flame retarding and electrochemically stable on both cathode and graphitic anode [134]. Numerous FRs have been investigated to lower the flammability of the liquid electrolytes. So far most of FR additives used in the liquid electrolytes are based on organic phosphorus compounds and their halogenated derivatives. Typical organic phosphorus compounds are trimethyl phosphate (TMP) [135–142], dimethyl methyl phosphonate (DMMP) [135,143–145], 4-isopropyl phenyl diphenyl phosphate (IPPP) [44,146–148], tris(2,2,2-trifluoroethyl) phosphite (TTFP) [149,150], triphenylphosphate (TPP) [151–153], cresyl diphenyl phosphate (CDP) [154–156], diphenyloctyl phosphate (DPOF) [150,157,158], alkyl phosphate [47,137,159,160], hexamethylphosphoramide (HMPA) [161], tributylphosphate (TBP) [152], tris(2,2,2-trifluoroethyl) phosphate(TFP) [134,160] and so on. On the other hand, fluorinated propylene carbonates [162,163] and methyl nonafluorobuyl ether (MFE) [164–166] have been studied as the non-phosphorus FR. Succinonitrile was reported as the electrolyte additive and can reduce the amount of gas emitted at high temperature, increase the onset temperature of exothermic reactions and decrease the amount of exothermal heat [167]. The reduction in flammability with the addition of these FRs has to be realized at an expense of the other performances such as ionic conductivity of the electrolyte and reversibility of the cell.

Since adding additive always bring some performances loss for the battery. Another way to improve the stability of electrolyte is to change the compounds of solvent and lithium salt, which also should be guaranteed has good compatibility with the electrodes. Lithium bis(oxalate)borate (LiBOB)/γ-butyrolactone (GBL) based electrolyte was proposed recently [168–171]. Ping et al. [168] found that the 1 M LiBOB/GBL + dimethyl sulfite (DMS) (3:1 wt.) electrolyte mitigates the irreversible capacity and enhances the first coulomb efficiency and the capacity retention. The thermal stability of LiBOB/GBL series electrolytes are improved greatly than that of $LiPF_6$/EC + DEC electrolyte as shown in Fig. 9 [168]. These beneficial effects make LiBOB/GBL possibly to be a promising alternative electrolyte for lithium ion battery.

5.1.5. Overcharge additive

According to the function, the overcharge protection additives can be classified as redox shuttle additive and shutdown additive

[133]. The former protects the cell from overcharge reversibly, while the latter terminates cell operation permanently.

The thianthrene derivatives [172], polysulfide [173], 2,5-ditertbutyl-1,4-dimethoxybenzene [174–179], polytriphenylamine [180–182], 4-tertbutyl-1,2-dimethoxybenzene [183], 3-chloroanisole (3CA) [184,185], 2,2,6,6-tetramethylpiperidine-1-oxyl (TEMPO) [186], diphenylamine [187] and so on were explored as redox shuttle additives. These soluble redox couples have been suggested as shuttles for overcharge protection, but they work only at high charging voltages, which means they actually do not respond to heat generation in batteries [12]. The shutdown additive will terminate cell operation permanently. The cyclohexyl benzene [14,188–192], biphenyl [153,185,193–195], xylene [196], cyclohexylbenzene [197] and the others have been investigated.

Nevertheless, given the paramount importance of safety, redox chemical shuttles, which can only provide limited overcharge protection and cannot prevent catastrophic failure as obtained during severe overcharging, shutdown protection mechanisms such as polymerizable additives must be incorporated even at the cost of termination of useful life of the battery [12].

5.2. Safety devices

The safety design for lithium ion battery is finding a way to release high pressure and heat before thermal runaway. Based on this ideal, safety vents, thermal fuse, positive temperature coefficient (PTC), shutdown separators and special battery management system (BMS) were developed for battery packs.

Prismatic cells swell and cylindrical cells bulge during pressurization and then safety vents are designed to release the internal pressure of the cell when a specified pressure is reached [198]. Swart et al. [198] discussed the various venting mechanisms employed by prismatic and cylindrical lithium ion cells and test methods to characterize the mechanical safety vent's opening pressure for both cylindrical and prismatic cells. But it should be noted that after the vent (or pressure-release rupture) is opened, the gas accumulating inside the cell will be released. After that, atmospheric air (with fresh oxygen and moisture) will enter the battery and react with the freshly plated lithium metal and electrolyte, causing explosion and ignition [199].

Thermal fuse is a wire of a fusible alloy with resistance and thermal characteristics that allow it to melt when a pre-set current flows through it. It will permanently shut down the battery if it is exposed to excessive temperatures. If the voltage is too high, the disconnection of the thermal fuse does not interrupt the thermal runaway of lithium [191]. Thermal fuses are employed as protection against thermal runaway and are usually set to open at 30–50 °C above the maximum operating temperature of the battery [12].

The PTC increases its resistivity at temperatures above its melting point. If a large current flows across the PTC element, its temperature rises up abruptly up due to Joule heat evolution within the PTC element. A concomitant and abnormally high resistance of the PTC element prevents current flow. Thus, upon activation, the resistance of the PTC element shoots up, leading to a precipitous fall in the current, which limits heat generation in the cell. The primary purpose of PTC devices is to protect batteries against external short circuits, and they also provide protection under certain other electrical abuse conditions [12].

The PTC mainly includes ceramic PTC and conductive-polymer PTC devices. Ceramic materials with fuse-like action are the materials of choice for early PTC elements. Conductive-polymer PTC devices are non-linear PTC thermistors based on a composite of polymers and conductive particles. These PTC may not be able to respond when the hazardous reactions happen at very high rate. And then, the PTC electrode were developed, which contains the PTC compound as the conductive material [200–202]. These PTC electrode exhibits normal electrochemical behaviors at ambient temperature, but shows an enormous increase in the resistance at the temperature range of 100–130 °C. This PTC behavior of the electrode provides a current-limiting effect, acting as a reversible thermal shutdown switch for rechargeable lithium batteries.

According to the structure and composition of the membranes, the battery separators can be broadly divided as three groups [203,204]: (1) microporous polymer membranes, (2) non-woven fabric mats and (3) inorganic composite membranes. In lithium ion batteries, the polyolefin microporous films are widely used, which are generally uniaxially drawn polyethylene (PE) and polypropylene (PP), biaxially drawn PE or multiaxially drawn PP/PE/PP. Among numerous battery separators, the thermal shutdown and ceramic separators are of special importance in enhancing the safety of lithium ion batteries. It is required to be capable of battery shutdown at the temperature below that at which thermal runaway occurs, and the shutdown should not result in loss of mechanical integrity [203]. It is validated that PE containing separators, in particular trilayer laminates of PP, PE and PP, appear to have the most attractive properties for preventing thermal runaway in lithium ion cells [205]. The PE–PP bilayer separators used currently in lithium ion batteries, and they have about 130 °C shutdown temperature and about 165 °C melting temperature. Chung et al. [206] coated PE with polymer synthesized from diethylene glycol dimethacrylate (DEGDMA), its shutdown temperature and meltdown temperature were improved to 142 °C and 155 °C, respectively, and a slight increase in the air permeability. Li et al. [182] modified the commercial Celgard separator with polytriphenylamine (PTPAn), and found this electroactive separator can reversibly control the cell's voltage at the safe value less than 4.15 V at high rate overcharge of 2 C current without obvious negative impact on the normal charge-discharge performances of the commercial $LiFePO_4$/C batteries even at prolonged overcharge cycling, showing a potential application in 3.6 V-class lithium ion batteries [182].

To provide safe operation and optimum performance, these large lithium ion battery packs must be supervised by an electronic BMS that monitors and services each of the individual cells. The features of a BMS depend on the application, but in most cases, features like data acquisition, battery state determination, electrical management and thermal management, safety management are necessary [207].

The rise of temperature in the cell depends strongly on cell, chemistry as well as discharge rate. Computer simulation of the cycling of scaled-up lithium ion batteries shows that the cell temperature profile also depends strongly on the surface cooling rate. An effective thermal management system is required to operate these batteries safely specifically for electric vehicle (EV)/HEV applications [208,209]. Plett proposed an extended Kalman filtering (EKF) method, to accomplish these goals on a lithium ion polymer battery pack [210–213]. The results were presented that demonstrate it is possible to achieve root-mean-squared modeling error smaller than the level of quantization error expected in an implementation [211].

Related works were performed on laptop battery packs and plug-in hybrid electric vehicle (PHEV) [214,215], and the active (air-cooled) and passive (phase change material, PCM) thermal management were compared. The results show that at stressful conditions, i.e. at high discharge rates and at high operating or ambient temperatures (for example 40–45 °C), air-cooling is not a proper thermal management system to keep the temperature of the cell in the desirable operating range without expending significant fan power. On the other hand, the cooling system is able to meet the operating range requirements under these same stressful conditions without the need for additional fan power [215].

6. Summary and outlook

With the global energy policy changing from fossil energy to renewable energy, we are taking more and more interest on wind energy, solar energy, EV/HEVs, and related energy storage technology. Lithium ion battery, as a kind of energy storage method shows great advantage over other kinds of battery. However, safety issue still is a main obstacle for the applications of large-size or high-rate lithium ion batteries in many high technology fields, such as electric vehicles and electric storage devices. With increasing interest in lithium-ion batteries for automotive applications, more investigations should be carried out to make the lithium ion battery safer and safer.

Safety issues related to thermal runaway is a very complicated process involving chemistry, material science and engineering, and it should be considered from electrode materials and electrolyte to cell design. The general thermal runaway theory was proposed and it is clear. However, many different electrode materials, electrolytes and cell types show different thermal runaway behaviors, and these exact reactions at different thermal runaway stages is under investigating, which are depending on the components materials, cathode, anode and electrolyte. The reactions also are dominated by the state of charge, discharging rate, etc. To disclose all of these reactions need our sustaining research.

The thermal models from one dimensional to three dimensional have been developed and simulated using FEM or FVM methods. These are simplified models and the three dimensional thermal-electrochemical model which covers the real conditions is necessary. More efficient thermal management based on single cell thermal model for cell pack used in EV and HEV is to be developed and simulated further, which should cover the thermal, electrochemical, and environmental conditions. The extreme conditions should be considered in the future work, especially for the EV and HEV applications, for example, the start of engine will generate high discharge rate, and the heat generation rate should be well modeled for the accurate prediction of thermal runaway.

The inherent safety method is the final way to solve the thermal runaway problem, but the balance between the electrochemical performances and thermal stability is a hard choice for us. The electrolyte, cathode and anode materials are critical for the thermal stability of battery. To develop a safe electrolyte with good electrochemical performance, compatibility with electrodes and thermal stability is still under developing. New generation rechargeable lithium batteries is under developing, such as, Li-alloy anode based Li-ion batteries, Li-metal anode-based rechargeable batteries, Li–air battery, Li–S battery and so on [216,217], and their thermal runaway risks are under investigating.

Coupling with the inherent safety method, using one or more safety devices is an efficient way to prevent the battery explosion at present. However, in the thermal runaway mechanism for varies battery systems, and the related thermal runaway prevention measures and BMS need be understood and developed further, especially for the EV and HEV applications.

Acknowledgements

This study is supported by the National Natural Science Foundation of China (Grant No. 51176183 and 70803015). Scientific Research Foundation for Returned Overseas Scholars, and the Fundamental Research Funds for the Central Universities (Grant no. WK2320000004), Ministry of Education of PR China.

References

[1] P. Poizot, F. Dolhem, Energy Environ. Sci. 4 (2011) 2003–2019.
[2] B. Scrosati, J. Garche, J. Power Sources 195 (2010) 2419–2430.
[3] J.Y. Lee, D. Deng, M.G. Kim, J. Cho, Energy Environ. Sci. 2 (2009) 818–837.
[4] T.M. Bandhauer, S. Garimella, T.F. Fuller, J. Electrochem. Soc. 158 (2011) R1–R25.
[5] J.B. Goodenough, Y. Kim, Chem. Mater. 22 (2010) 587–603.
[6] J.M. Tarascon, M. Armand, Nature 414 (2001) 359–367.
[7] Y. Nishi, Chem. Rec. 1 (2001) 406–413.
[8] M. Wakihara, Mater. Sci. Eng. Rep. 33 (2001) 109–134.
[9] V. Etacheri, R. Marom, R. Elazari, G. Salitra, D. Aurbach, Energy Environ. Sci. 4 (2011) 3243–3262.
[10] ScienceDaily, American Chemical Society, 2007, http://www.sciencedaily.com/releases/2007/2012/071217110106.htm.
[11] E. Peter, L. Alan, USA, TODAY, Washington, 2007.
[12] P.G. Balakrishnan, R. Ramesh, T.P. Kumar, J. Power Sources 155 (2006) 401–414.
[13] Rutgers University, New Brunswick, 2006.
[14] S.Y. Chen, Z.X. Wang, H.L. Zhao, L.Q. Chen, Prog. Chem. 21 (2009) 629–636.
[15] F. Torabi, V. Esfahanian, J. Electrochem. Soc. 158 (2011) A850–A858.
[16] R.M. Spotnitz, J. Weaver, G. Yeduvaka, D.H. Doughty, E.P. Roth, J. Power Sources 163 (2007) 1080–1086.
[17] B.K. Mandal, A.K. Padhi, Z. Shi, S. Chakraborty, R. Filler, J. Power Sources 161 (2006) 1341–1345.
[18] A. Hammami, N. Raymond, M. Armand, Nature 424 (2003) 635–636.
[19] Q.S. Wang, P. Ping, J.H. Sun, Nonlinear Dynam. 61 (2010) 763–772.
[20] K. Kumaresan, G. Sikha, R.E. White, J. Electrochem. Soc. 155 (2008) A164–A171.
[21] Q.S. Wang, J.H. Sun, G.Q. Chu, Fire Safety Science – Proceedings of the Eighth International Symposium International Association for Fire Safety Science, Beijing, 2005, pp. 375–382.
[22] G.H. Kim, A. Pesaran, R. Spotnitz, J. Power Sources 170 (2007) 476–489.
[23] R. Spotnitz, J. Franklin, J. Power Sources 113 (2003) 81–100.
[24] N.N. Semenov, Some Problems in Chemical Kinetics in Reactivity, Princeton University Press, New Jersey, 1959.
[25] Y.F. Chen, J.W. Evans, J. Electrochem. Soc. 143 (1996) 2708–2712.
[26] W.B. Gu, C.Y. Wang, J. Electrochem. Soc. 147 (2000) 2910–2922.
[27] T.D. Hatchard, D.D. MacNeil, A. Basu, J.R. Dahn, J. Electrochem. Soc. 148 (2001) A755–A761.
[28] D.H. Doughty, P.C. Butler, R.G. Jungst, E.P. Roth, J. Power Sources 110 (2002) 357–363.
[29] P.M. Gomadam, R.E. White, J.W. Weidner, J. Electrochem. Soc. 150 (2003) A1339–A1345.
[30] J. Newman, K.E. Thomas, H. Hafezi, D.R. Wheeler, J. Power Sources 119 (2003) 838–843.
[31] S.C. Chen, C.C. Wan, Y.Y. Wang, J. Power Sources 140 (2005) 111–124.
[32] C. Forgez, D.V. Do, G. Friedrich, M. Morcrette, C. Delacourt, J. Power Sources 195 (2010) 2961–2968.
[33] L. Menard, G. Fontes, S. Astier, Math. Comput. Simulat. 81 (2010) 327–339.
[34] R.E. Gerver, J.P. Meyers, J. Electrochem. Soc. 158 (2011) A835–A843.
[35] X.W. Zhang, Electrochim. Acta 56 (2011) 1246–1255.
[36] K. Onda, T. Ohshima, M. Nakayama, K. Fukuda, T. Araki, J. Power Sources 158 (2006) 535–542.
[37] L.W. Zhao, I. Watanabe, T. Doi, S. Okada, J. Yamaki, J. Power Sources 161 (2006) 1275–1280.
[38] I. Watanabe, J. Yamaki, J. Power Sources 153 (2006) 402–404.
[39] Q.S. Wang, J.H. Sun, X.L. Yao, C.H. Chen, J. Electrochem. Soc. 153 (2006) A329–A333.
[40] J. Yamaki, H. Takatsuji, T. Kawamura, M. Egashira, Solid State Ionics 148 (2002) 241–245.
[41] A.M. Andersson, K. Edstrom, N. Rao, A. Wendsjo, J. Power Sources 82 (1999) 286–290.
[42] D. Aurbach, A. Zaban, Y. Ein-Eli, I. Weissman, O. Chusid, B. Markovsky, M. Levi, E. Levi, A. Schechter, E. Granot, J. Power Sources 68 (1997) 91–98.
[43] Q.S. Wang, J.H. Sun, X.L. Yao, C.H. Chen, Thermochim. Acta 437 (2005) 12–16.
[44] Q.S. Wang, J.H. Sun, Mater. Lett. 61 (2007) 3338–3340.
[45] G. Venugopal, J. Power Sources 101 (2001) 231–237.
[46] Q.S. Wang, J.H. Sun, X.F. Chen, G.Q. Chu, C.H. Chen, Mater. Res. Bull. 44 (2009) 543–548.
[47] Y. Shigematsu, M. Ue, J. Yamaki, J. Electrochem. Soc. 156 (2009) A176–A180.
[48] S.Y. Lee, S.K. Kim, S. Ahn, J. Power Sources 174 (2007) 480–483.
[49] J. Jiang, J.R. Dahn, Electrochim. Acta 49 (2004) 2661–2666.
[50] J. Yamaki, Y. Baba, N. Katayama, H. Takatsuji, M. Egashira, S. Okada, J. Power Sources 119 (2003) 789–793.
[51] H. Yang, X.D. Shen, J. Power Sources 167 (2007) 515–519.
[52] J.S. Gnanaraj, E. Zinigrad, L. Asraf, H.E. Gottlieb, M. Sprecher, D. Aurbach, M. Schmidt, J. Power Sources 119 (2003) 794–798.
[53] T. Kawamura, A. Kimura, M. Egashira, S. Okada, J.I. Yamaki, J. Power Sources 104 (2002) 260–264.
[54] M. Moshkovich, M. Cojocaru, H.E. Gottlieb, D. Aurbach, J. Electroanal. Chem. 497 (2001) 84–96.
[55] E. Markevich, G. Salitra, D. Aurbach, Electrochem. Commun. 7 (2005) 1298–1304.
[56] R. Marom, S.F. Amalraj, N. Leifer, D. Jacob, D. Aurbach, J. Mater. Chem. 21 (2011) 9938–9954.
[57] A. Du Pasquier, F. Disma, T. Bowmer, A.S. Gozdz, G. Amatucci, J.M. Tarascon, J. Electrochem. Soc. 145 (1998) 472–477.
[58] F.M. Gray, Solid Polymer Electrolytes: Fundamentals and Technological Applications, VCH, 1991.

[59] M.N. Richard, J.R. Dahn, J. Power Sources 79 (1999) 135–142.
[60] G. Nagasubramanian, D. Ingersoll, D. Doughty, D. Radzykewycz, C. Hill, C. Marsh, J. Power Sources 80 (1999) 116–118.
[61] E.P. Roth, D.H. Doughty, J. Power Sources 128 (2004) 308–318.
[62] S. Al Hallaj, H. Maleki, J.S. Hong, J.R. Selman, J. Power Sources 83 (1999) 1–8.
[63] C.R. Pals, J. Newman, J. Electrochem. Soc. 142 (1995) 3274–3281.
[64] C.R. Pals, J. Newman, J. Electrochem. Soc. 142 (1995) 3282–3288.
[65] K. Smith, C.Y. Wang, J. Power Sources 160 (2006) 662–673.
[66] G.G. Botte, B.A. Johnson, R.E. White, J. Electrochem. Soc. 146 (1999) 914–923.
[67] G.G. Botte, V.R. Subramanian, R.E. White, Electrochim. Acta 45 (2000) 2595–2609.
[68] U.S. Kim, C.B. Shin, C.S. Kim, J. Power Sources 180 (2008) 909–916.
[69] S.C. Chen, Y.Y. Wang, C.C. Wan, J. Electrochem. Soc. 153 (2006) A637–A648.
[70] L. Song, J.W. Evans, J. Electrochem. Soc. 147 (2000) 2086–2095.
[71] V. Srinivasan, C.Y. Wang, J. Electrochem. Soc. 150 (2003) A98–A106.
[72] M. Sievers, U. Sievers, S.S. Mao, Forsch. Ingenieurwes. 74 (2010) 215–231.
[73] D.R. Baker, M.W. Verbrugge, J. Electrochem. Soc. 146 (1999) 2413–2424.
[74] Y.F. Chen, J.W. Evans, J. Electrochem. Soc. 141 (1994) 2947–2955.
[75] G.F. Guo, B. Long, B. Cheng, S.Q. Zhou, P. Xu, B.G. Cao, J. Power Sources 195 (2010) 2393–2398.
[76] D.H. Jeon, S.M. Baek, Energy Convers. Manage. 52 (2011) 2973–2981.
[77] M. Guo, G. Sikha, R.E. White, J. Electrochem. Soc. 158 (2011) A122–A132.
[78] K. Smith, G.H. Kim, E. Darcy, A. Pesaran, Int. J. Energy Res. 34 (2010) 204–215.
[79] S. Santhanagopalan, P. Ramadass, J. Zhang, J. Power Sources 194 (2009) 550–557.
[80] L. Cai, R.E. White, J. Electrochem. Soc. 157 (2010) A1188–A1195.
[81] W.F. Fang, O.J. Kwon, C.Y. Wang, Int. J. Energy Res. 34 (2010) 107–115.
[82] S. Santhanagopalan, Q.Z. Guo, P. Ramadass, R.E. White, J. Power Sources 156 (2006) 620–628.
[83] L. Cai, R.E. White, J. Power Sources 196 (2011) 5985–5989.
[84] S. Santhanagopalan, R.E. White, Int. J. Energy Res. 34 (2010) 152–163.
[85] M.W. Verbrugge, AIChE J. 41 (1995) 1550–1562.
[86] S. Bhide, T. Shim, IEEE Trans. Veh. Technol. 60 (2011) 819–829.
[87] L.J. Gao, S.Y. Liu, R.A. Dougal, IEEE Trans. Compon. Pack. Technol. 25 (2002) 495–505.
[88] Y. Hu, S. Yurkovich, Y. Guezennec, B.J. Yurkovich, J. Power Sources 196 (2011) 449–457.
[89] R. Mahamud, C. Park, J. Power Sources 196 (2011) 5685–5696.
[90] S.A. Khateeb, M.M. Farid, J.R. Selman, S. Al-Hallaj, J. Power Sources 158 (2006) 673–678.
[91] M.S. Wu, K.H. Liu, Y.Y. Wang, C.C. Wan, J. Power Sources 109 (2002) 160–166.
[92] G.C.S. Freitas, F.C. Peixoto, A.S. Vianna, J. Power Sources 179 (2008) 424–429.
[93] U.S. Kim, J. Yi, C.B. Shin, T. Han, S. Park, J. Power Sources 196 (2011) 5115–5121.
[94] U.S. Kim, J. Yi, C.B. Shin, T. Han, S. Park, J. Electrochem. Soc. 158 (2011) A611–A618.
[95] S. Kim, Y.S. Lee, H.S. Lee, H.L. Jin, Materialwiss. Werkstofftech. 41 (2010) 378–385.
[96] S. Tobishima, J. Yamaki, J. Power Sources 82 (1999) 882–886.
[97] K. Kitoh, H. Nemoto, J. Power Sources 82 (1999) 887–890.
[98] S. Tobishima, K. Takei, Y. Sakurai, J. Yamaki, J. Power Sources 90 (2000) 188–195.
[99] C.J. Orendorff, E.P. Roth, G. Nagasubramanian, J. Power Sources 196 (2011) 6554–6558.
[100] R.A. Leising, M.J. Palazzo, E.S. Takeuchi, K.J. Takeuchi, J. Electrochem. Soc. 148 (2001) A838–A844.
[101] R.A. Leising, M.J. Palazzo, E.S. Takeuchi, K.J. Takeuchi, J. Power Sources 97 (8) (2001) 681–683.
[102] C.H. Doh, D.H. Kim, H.S. Kim, H.M. Shin, Y.D. Jeong, S.I. Moon, B.S. Jin, S.W. Eom, H.S. Kim, K.W. Kim, D.H. Oh, A. Veluchamy, J. Power Sources 175 (2008) 881–885.
[103] T. Ohsaki, T. Kishi, T. Kuboki, N. Takami, N. Shimura, Y. Sato, M. Sekino, A. Satoh, J. Power Sources 146 (2005) 97–100.
[104] Y. Saito, K. Takano, A. Negishi, J. Power Sources 97 (8) (2001) 693–696.
[105] H.Y. Wang, A.D. Tang, K.L. Huang, Chin. J. Chem. 29 (2011) 27–32.
[106] P. Ribiere, S. Grugeon, M. Morcrette, S. Boyanov, S. Laruelle, G. Marlair, Energy Environ. Sci. 5 (2012) 5271–5280.
[107] C. Mikolajczak, M. Kahn, K. White, R.T. Long, Exponent Failure Analysis Associates, Inc., Menlo Park, 2011, p. 125.
[108] C. Li, H.P. Zhang, L.J. Fu, H. Liu, Y.P. Wu, E. Ram, R. Holze, H.Q. Wu, Electrochim. Acta 51 (2006) 3872–3883.
[109] Y.H. Chen, Z.Y. Tang, G.Q. Zhang, X.M. Zhang, R.Z. Chen, Y.G. Liu, Q. Liu, J. Wuhan Univ. Technol. 24 (2009) 347–353.
[110] Z.X. Yang, W.S. Yang, D.G. Evans, G. Li, Y.Y. Zhao, Electrochem. Commun. 10 (2008) 1136–1139.
[111] W. Hong, M.C. Chen, Electrochem. Solid State 9 (2006) A82–A85.
[112] G.T.K. Fey, C.Z. Lu, T.P. Kumar, Y.C. Chang, Surf. Coat. Technol. 199 (2005) 22–31.
[113] R. Vidu, P. Stroeve, Ind. Eng. Chem. Res. 43 (2004) 3314–3324.
[114] J. Cho, T.J. Kim, J. Kim, M. Noh, B. Park, J. Electrochem. Soc. 151 (2004) A1899–A1904.
[115] J. Cho, Y.W. Kim, B. Kim, J.G. Lee, B. Park, Angew. Chem. Int. Ed. 42 (2003) 1618–1621.
[116] H.J. Kweon, J. Park, J. Seo, G. Kim, B. Jung, H.S. Lim, J. Power Sources 126 (2004) 156–162.
[117] L.X. Yuan, Z.H. Wang, W.X. Zhang, X.L. Hu, J.T. Chen, Y.H. Huang, J.B. Goodenough, Energy Environ. Sci. 4 (2011) 269–284.
[118] O.K. Park, Y. Cho, S. Lee, H.C. Yoo, H.K. Song, J. Cho, Energy Environ. Sci. 4 (2011) 1621–1633.
[119] Y.G. Wang, P. He, H.S. Zhou, Energy Environ. Sci. 4 (2011) 805–817.
[120] B. Kang, G. Ceder, Nature 458 (2009) 190–193.
[121] G.Y. Chen, T.J. Richardson, J. Power Sources 195 (2010) 1221–1224.
[122] D. Choi, J. Xiao, Y.J. Choi, J.S. Hardy, M. Vijayakumar, M.S. Bhuvaneswari, J. Liu, W. Xu, W. Wang, Z. Yang, G.L. Graff, J.-G. Zhang, Energy Environ. Sci. 4 (2011) 4560–4566.
[123] L. Xia, S.L. Li, X.P. Ai, H.X. Yang, Y.L. Cao, Energy Environ. Sci. 4 (2011) 2845–2848.
[124] Z.H. Chen, Y. Qin, Y. Ren, W.Q. Lu, C. Orendorff, E.P. Roth, K. Amine, Energy Environ. Sci. 4 (2011) 4023–4030.
[125] L.J. Fu, H. Liu, C. Li, Y.P. Wu, E. Rahm, R. Holze, H.Q. Wu, Solid State Sci. 8 (2006) 113–128.
[126] Y.S. Park, H.J. Bang, S.M. Oh, Y.K. Sun, S.M. Lee, J. Power Sources 190 (2009) 553–557.
[127] M.C. Zhao, M.M. Xu, H.D. Dewald, R.J. Staniewicz, J. Electrochem. Soc. 150 (2003) A117–A120.
[128] X.G. Sun, S. Dai, J. Power Sources 195 (2010) 4266–4271.
[129] H.Y. Lee, J.K. Baek, S.M. Lee, H.K. Park, K.Y. Lee, M.H. Kim, J. Power Sources 128 (2004) 61–66.
[130] T. Tsumura, A. Katanosaka, I. Souma, T. Ono, Y. Aihara, J. Kuratomi, M. Inagaki, Solid State Ionics 135 (2000) 209–212.
[131] Y.W. Zhu, S. Murali, M.D. Stoller, K.J. Ganesh, W.W. Cai, P.J. Ferreira, A. Pirkle, R.M. Wallace, K.A. Cychosz, M. Thommes, D. Su, E.A. Stach, R.S. Ruoff, Science 332 (2011) 1537–1541.
[132] I. Kovalenko, B. Zdyrko, A. Magasinski, B. Hertzberg, Z. Milicev, R. Burtovyy, I. Luzinov, G. Yushin, Science 333 (2011) 75–79.
[133] S.S. Zhang, J. Power Sources 162 (2006) 1379–1394.
[134] K. Xu, S.S. Zhang, J.L. Allen, T.R. Jow, J. Electrochem. Soc. 149 (2002) A1079–A1082.
[135] H.F. Xiang, H.W. Lin, B. Yin, C.P. Zhang, X.W. Ge, C.H. Chen, J. Power Sources 195 (2010) 335–340.
[136] D. Kam, K. Kim, H.S. Kim, H.K. Liu, Electrochem. Commun. 11 (2009) 1657–1660.
[137] N. Yoshimoto, Y. Niida, M. Egashira, M. Morita, J. Power Sources 163 (2006) 238–242.
[138] H.Y. Xu, S. Xie, Q.Y. Wang, X.L. Yao, Q.S. Wang, C.H. Chen, Electrochim. Acta 52 (2006) 636–642.
[139] X.M. Wang, C. Yamada, H. Naito, G. Segami, K. Kibe, J. Electrochem. Soc. 153 (2006) A135–A139.
[140] X.L. Yao, S. Xie, C.H. Chen, Q.S. Wang, J.H. Sun, Y.L. Li, S.X. Lu, J. Power Sources 144 (2005) 170–175.
[141] C.Y. Hu, X.H. Li, Trans. Nonferr. Metal Soc. 15 (2005) 1380–1387.
[142] H. Ota, A. Kominato, W.J. Chun, E. Yasukawa, S. Kasuya, J. Power Sources 119 (2003) 393–398.
[143] H.F. Xiang, Q.Y. Jin, R. Wang, C.H. Chen, X.W. Ge, J. Power Sources 179 (2008) 351–356.
[144] H.F. Xiang, H.Y. Xu, Z.Z. Wang, C.H. Chen, J. Power Sources 173 (2007) 562–564.
[145] H.F. Xiang, Q.Y. Jin, C.H. Chen, X.W. Ge, S. Guo, J.H. Sun, J. Power Sources 174 (2007) 335–341.
[146] Q.S. Wang, J.H. Sun, C.H. Chen, J. Power Sources 162 (2006) 1363–1366.
[147] Q.S. Wang, J.H. Sun, C.H. Chen, J. Appl. Electrochem. 39 (2009) 1105–1110.
[148] Q.S. Wang, J.H. Sun, X.L. Yao, C.H. Chen, Electrochem. Solid State 8 (2005) A467–A470.
[149] S.S. Zhang, K. Xu, T.R. Jow, J. Power Sources 113 (2003) 166–172.
[150] T.H. Nam, E.G. Shim, J.G. Kim, H.S. Kim, S.I. Moon, J. Power Sources 180 (2008) 561–567.
[151] E.G. Shim, T.H. Nam, J.G. Kim, H.S. Kim, S.I. Moon, Electrochim. Acta 53 (2007) 650–656.
[152] Y.E. Hyung, D.R. Vissers, K. Amine, J. Power Sources 119 (2003) 383–387.
[153] T.H. Nam, E.G. Shim, J.G. Kim, H.S. Kim, S.I. Moon, J. Electrochem. Soc. 154 (2007) A957–A963.
[154] Q.S. Wang, P. Ping, J.H. Sun, C.H. Chen, J. Power Sources 195 (2010) 7457–7461.
[155] E.G. Shim, T.H. Nam, J.G. Kim, H.S. Kim, S.I. Moon, Met. Mater. Int. 15 (2009) 615–621.
[156] D.Y. Zhou, W.S. Li, C.L. Tan, X.X. Zuo, Y.J. Huang, J. Power Sources 184 (2008) 589–592.
[157] E.G. Shim, T.H. Nam, J.G. Kim, H.S. Kim, S.I. Moon, Electrochim. Acta 54 (2009) 2276–2283.
[158] E.G. Shim, T.H. Nam, J.G. Kim, H.S. Kim, S.I. Moon, J. Power Sources 175 (2008) 533–539.
[159] K. Xu, S.S. Zhang, J.L. Allen, T.R. Jow, J. Electrochem. Soc. 150 (2003) A170–A175.
[160] K. Xu, M.S. Ding, S.S. Zhang, J.L. Allen, T.R. Jow, J. Electrochem. Soc. 150 (2003) A161–A169.
[161] S. Izquierdo-Gonzales, W.T. Li, B.L. Lucht, J. Power Sources 135 (2004) 291–296.
[162] M. Hasegawa, H. Ishii, Y. Cao, T. Fuchigami, J. Electrochem. Soc. 153 (2006) D162–D166.
[163] D.H. Jang, S.M. Oh, J. Electrochem. Soc. 144 (1997) 3342–3348.
[164] J. Arai, J. Electrochem. Soc. 150 (2003) A219–A228.
[165] J. Arai, H. Katayama, H. Akahoshi, J. Electrochem. Soc. 149 (2002) A217–A226.
[166] J. Arai, J. Appl. Electrochem. 32 (2002) 1071–1079.
[167] Y.-S. Kim, T.-H. Kim, H. Lee, H.-K. Song, Energy Environ. Sci. 4 (2011) 4038–4045.

[168] P. Ping, Q.S. Wang, J.H. Sun, X.Y. Feng, C.H. Chen, J. Power Sources 196 (2011) 776–783.
[169] D.T. Shieh, P.H. Hsieh, M.H. Yang, J. Power Sources 174 (2007) 663–667.
[170] Z.H. Chen, W.Q. Lu, J. Liu, K. Amine, Electrochim. Acta 51 (2006) 3322–3326.
[171] K. Xu, S.S. Zhang, U. Lee, J.L. Allen, T.R. Jow, J. Power Sources 146 (2005) 79–85.
[172] D.Y. Lee, H.S. Lee, H.S. Kim, H.Y. Sun, D.Y. Seung, Korean J. Chem. Eng. 19 (2002) 645–652.
[173] Y.V. Mikhaylik, J.R. Akridge, J. Electrochem. Soc. 151 (2004) A1969–A1976.
[174] J. Chen, C. Buhrmester, J.R. Dahn, Electrochem. Solid State 8 (2005) A59–A62.
[175] J.R. Dahn, J.W. Jiang, L.M. Moshurchak, M.D. Fleischauer, C. Buhrmester, L.J. Krause, J. Electrochem. Soc. 152 (2005) A1283–A1289.
[176] L.M. Moshurchak, C. Buhrmester, J.R. Dahn, J. Electrochem. Soc. 152 (2005) A1279–A1282.
[177] Z. Chen, K. Amine, Electrochim. Acta 53 (2007) 453–458.
[178] L.M. Moshurchak, C. Buhrmester, R.L. Wang, J.R. Dahn, Electrochim. Acta 52 (2007) 3779–3784.
[179] M. Taggougui, B. Carre, P. Willmann, D. Lemordant, J. Power Sources 174 (2007) 1069–1073.
[180] J.K. Feng, X.P. Ai, Y.L. Cao, H.X. Yang, J. Power Sources 161 (2006) 545–549.
[181] X.M. Feng, J.Y. Zheng, J.J. Zhang, R.F. Li, Z.J. Li, Electrochim. Acta 54 (2009) 4036–4039.
[182] S.L. Li, X.P. Ai, H.X. Yang, Y.L. Cao, J. Power Sources 189 (2009) 771–774.
[183] J.K. Feng, X.P. Ai, Y.L. Cao, H.X. Yang, Electrochem. Commun. 9 (2007) 25–30.
[184] Y.G. Lee, J. Cho, Electrochim. Acta 52 (2007) 7404–7408.
[185] B.A. Zeng, S.Q. Liu, K.L. Huang, H.Y. Wang, J.H. Huang, J.S. Liu, Acta Chim. Sin. 67 (2009) 2815–2821.
[186] M. Taggougui, B. Carre, P. Willmann, D. Lemordant, J. Power Sources 174 (2007) 643–647.
[187] S.L. Li, X.P. Ai, J.K. Feng, Y.L. Cao, H.X. Yang, J. Power Sources 184 (2008) 553–556.
[188] H. Lee, J.H. Lee, S. Ahn, H.J. Kim, J.J. Cho, Electrochem. Solid State 9 (2006) A307–A310.
[189] Y.B. He, Q. Liu, Z.Y. Tang, Y.H. Chen, Q.S. Song, Electrochim. Acta 52 (2007) 3534–3540.
[190] H. Lee, S. Kim, J. Jeon, J.J. Cho, J. Power Sources 173 (2007) 972–978.
[191] Y.S. Chen, C.C. Hu, Y.Y. Li, J. Power Sources 181 (2008) 69–73.
[192] M.Q. Xu, L.D. Xing, W.S. Li, X.X. Zuo, D. Shu, G.L. Li, J. Power Sources 184 (2008) 427–431.
[193] L.F. Xiao, X.P. Ai, Y.L. Cao, H.X. Yang, Electrochim. Acta 49 (2004) 4189–4196.
[194] S.J. Choi, S.M. Park, J. Electrochem. Soc. 155 (2008) A783–A787.
[195] K. Abe, Y. Ushigoe, H. Yoshitake, M. Yoshio, J. Power Sources 153 (2006) 328–335.
[196] Q.Y. Zhang, C.C. Qiu, Y.B. Fu, X.H. Ma, Chin. J. Chem. 27 (2009) 1459–1463.
[197] G.E. Blomgren, J. Power Sources 119 (2003) 326–329.
[198] J. Swart, A. Arora, M. Megerle, S. Nilsson, Product Safety Engineering Society Symposium, 2006 IEEE, 2006, pp. 1–4.
[199] D. Belov, M.H. Yang, J. Solid State Electrochem. 12 (2008) 885–894.
[200] X.M. Feng, X.P. Ai, H.X. Yang, Electrochem. Commun. 6 (2004) 1021–1024.
[201] M. Kise, S. Yoshioka, K. Hamano, H. Kuriki, T. Nishimura, H. Urushibata, H. Yoshiyasu, J. Electrochem. Soc. 152 (2005) A1516–A1520.
[202] M. Kise, S. Yoshioka, H. Kuriki, J. Power Sources 174 (2007) 861–866.
[203] S.S. Zhang, J. Power Sources 164 (2007) 351–364.
[204] Y. Wang, H.Y. Zhan, J. Hu, Y. Liang, S.S. Zeng, J. Power Sources 189 (2009) 616–619.
[205] G. Venugopal, J. Moore, J. Howard, S. Pendalwar, J. Power Sources 77 (1999) 34–41.
[206] Y.S. Chung, S.H. Yoo, C.K. Kim, Ind. Eng. Chem. Res. 48 (2009) 4346–4351.
[207] A. Jossen, V. Spath, H. Doring, J. Garche, J. Power Sources 84 (1999) 283–286.
[208] J.R. Selman, S. Al Hallaj, I. Uchida, Y. Hirano, J. Power Sources 97 (8) (2001) 726–732.
[209] S. Al-Hallaj, J.R. Selman, J. Power Sources 110 (2002) 341–348.
[210] G.L. Plett, J. Power Sources 134 (2004) 252–261.
[211] G.L. Plett, J. Power Sources 134 (2004) 262–276.
[212] G.L. Plett, J. Power Sources 134 (2004) 277–292.
[213] G.L. Plett, J. Power Sources 161 (2006) 1369–1384.
[214] A. Mills, S. Al-Hallaj, J. Power Sources 141 (2005) 307–315.
[215] R. Sabbah, R. Kizilel, J.R. Selman, S. Al-Hallaj, J. Power Sources 182 (2008) 630–638.
[216] G. Jeong, Y.U. Kim, H. Kim, Y.J. Kim, H.J. Sohn, Energy Environ. Sci. 4 (2011) 1986–2002.
[217] B. Scrosati, J. Hassoun, Y.K. Sun, Energy Environ. Sci. 4 (2011) 3287–3295.